UNIVERSITY OF ANTWERP

Faculty of applied engineering sciences: electromechanics

Bachelor's thesis submitted to obtain the degree of Bachelor in Electromechanical Engineering

Academic year 2023-2024

Analysis of an Organic Rankine Cycle for a Low to Medium Temperature Range applied to a Geothermal Energy Source

By Robbe Meysmans & Willem Vandenhove

Contents

Abstract 5
1. Case study 6
2. Literature Review 7
2.1. Organic Rankine cycle 7
2.1.1. Idealised thermodynamic cycle 7
2.1.2. Comparisson Rankine cycle – organic Rankine cycle 8
2.1.3. Real-world behavior of an ORC 9
2.2. Working Fluids 11
2.2.1. Classifying working fluids by its saturated vapour curve 11
2.2.2. Thermodynamical properties of working fluids 12
2.2.3. Environmental and safety considerations 13
2.2.4. Summary on working fluids 13
2.3. Different cycle designs 14
2.3.1. Sub-and super critical cycle designs 14
2.3.2. Multi-pressure level cycle designs 15
2.5. Analysis of main components 15
2.5.1. Expander 15
2.5.1.1. General overview 15
2.5.1.2 Thermodynamics of a radial inflow turbine 15
2.5.2. Heat exchangers 16
2.5.2.1. General overview 16
2.5.2.2. Fouling factor and cross flow correction factor 17
2.5.2.3. Exergy destruction in heat exchangers 18
2.5.2.4. The pinch point 19
2.5.2.5. Pressure drops in a shell and tube heat exchanger 20
2.5.3. Pump 20
2.5.4. Piping system 21
2.6. Geothermal energy 22
2.6.1. Geothermal heat generation 22
2.6.2. Geothermal heat sources 22
2.6.3. Geothermal power generation 23
3. Methodology 24
3.1. Overview 24

3.2. Simulation tools 24
3.3. Model 25
3.3.1. Baseline model 25
3.3.2. Model with recuperator 25
3.3.3. Pinch point and heat exchanger sizing 25
3.3.4. Heat exchanger losses and piping losses 25
3.3.5. Assesment criteria 25
4. Results 26
4.1. Initial selection of working fluids 26
4.2. Baseline model 26
4.3. Model with recuperator and working fluid selection 29
4.4. Effect of heat exchanger losses, piping losses and pinch point 31
4.5. Heat exchanger size & cycle efficiency 32
4.6. Sensitivity analysis 34
4.7. Validation and limitations 35
5. Conclusions 35
6. References 36
8. Appendices 43
A. Key thermodynamic concepts 43
A.a. Thermodynamic heat engine 43
A.b. The Carnot cycle and Second-law analysis 44
A.c. The Rankine cycle 45
B. Working fluids 47
B.a. ODP and GWP 47
B.b. Other environmental considerations 47
B.c. Techno-economic selection of working fluids 47
C. Other ORC energy sources 48
C.a. Concentrated solar power 48
C.b. Waste heat 49

Abstract

More and more people are faced with the effects of global warming in their day-to-day lives. This fact, alongside the ever-growing world's energy demand, creates an increasing need for the efficient use of different energy resources. The low-temperature heat-conversion technology of the Organic Rankine Cycle (ORC) can help fulfil this need by contributing its share towards a carbon and climate neutral future and by improving the efficient use of already available energy resources. ORC's transform low-temperature heat into useful work, making it possible to use renewable heat energy sources such as concentrated solar, geothermal heat and waste heat.

The organic Rankine cycle is a thermodynamic cycle that is derived from the Rankine cycle. The Rankine Cycle, a fundamental cycle in thermodynamics, serves as the cornerstone for a vast majority of power generation systems. This cycle, characterized by its four-stage process of pressurisation, heat addition, expansion, and heat rejection, forms the basis for most high power steam power plants worldwide. The organic Rankine cycle is similar in design but differs in some key parts of its execution. First, organic Rankine cycles use an organic compound as the working fluid instead of water. Second, organic Rankine cycles operate at much lower temperatures than Rankine cycles. And third, organic Rankine cycles can be much smaller in size and be built for smaller power applications. Because of these reasons, ORC's are an excellent candidate for a plethora of renewable sources.

In this paper, the organic Rankine cycle is applied to the renewable energy source of geothermal energy. The goal of the analysis is to determine a realistic cycle efficiency of such an ORC, using an optimal working fluid. Furthermore, some additional exploration on the sizing of components with respect to the cycle efficiency is carried out. To do so, the literature on the subject is thoroughly explored. In the exploration of the literature, first, the general theoretical backbone of ORC is examined. Next, the large range of working fluids are investigated and their efficiencies and environmental/health impact assessed. Then, the different cycle designs are discussed. Afterwards, the different key components of the cycle are considered. And finally, the applications of ORC are looked into, with special attention given to geothermal energy.

From this literature study, the baseline parameters for an ORC model using a geothermal heat source are derived (a heat source temperature of 150°C, a heat sink temperature of 12°C, a mass flow rate of 10 kg/s and a mechanical power output 400 kW). Then, a baseline model is constructed with the key building blocks of an ORC, namely: a pump, an expander, a condenser and an evaporator. Afterwards, the baseline model is expanded by considering the recuperator in the heat-regeneration cycle. Next, additional real-world considerations are added by looking at losses due to friction, heat transfer, and entropy increases in the expander and heat exchanger. Then, an optimal working fluid is selected using the real-world model by considering cycle efficiency, environmental impact and health-and safety concerns. In addition, the trade-off between cycle efficiency and installation sizing is discussed. Finally, a sensitivity analysis is carried out to act as a robustness check on the results and the effect of a variable heat source is considered.

The results of the analysis show that, from a techno-economic standpoint, the most optimal cycle has a cycle efficiency of 19%. This was achieved by using isobutane (R600a) as a working fluid, with turbine inlet and outlet temperature and pressure of 145 °C and 30 bar, and 73 °C and 3.5 bar, respectively.

1. Case study

A geothermal power plant is considered in which an organic Rankine cycle (ORC) is used to generate electrical power from a thermal heat source. The geothermal power plant uses a dry-rock heat reservoir to heat water to 150°C with a mass flow rate of 10 kg/s and extracts its energy to power a turbine that produces 400 kW of mechanical power. The heat sink is assumed to be a nearby river close to the power plant, with a constant temperature of 12°C. A diagram of the examined power cycle is shown in figure 1. The goal of this paper is to model the complete cycle, examine its cycle efficiencies given several real world considerations (such as pressure drops and heat losses), and compare and select optimal working fluids for the cycle. In addition, the trade-off between cycle efficiency and installation cost is discussed by looking at heat exchanger sizing and its effect on cycle performance. Furthermore, a sensitivity analysis is carried out on the main results of the paper.

To achieve these goals, an extended literature review on the different topics is carried out to build an accurate model of an ORC. First, the organic Rankine cycle is discussed and its key differences with the Rankine cycle are highlighted. Afterwards, different cycle designs and working fluid characteristics are examined. Next, the main components of the ORC are discussed in greater detail, to allow for accurate modelling of the cycle in the case study. And finally, a brief overview of possible applications is given, with special attention given to geothermal power. The different topics presented in the literature review are then used for the modelling of an ORC to help achieve the goals of the paper.

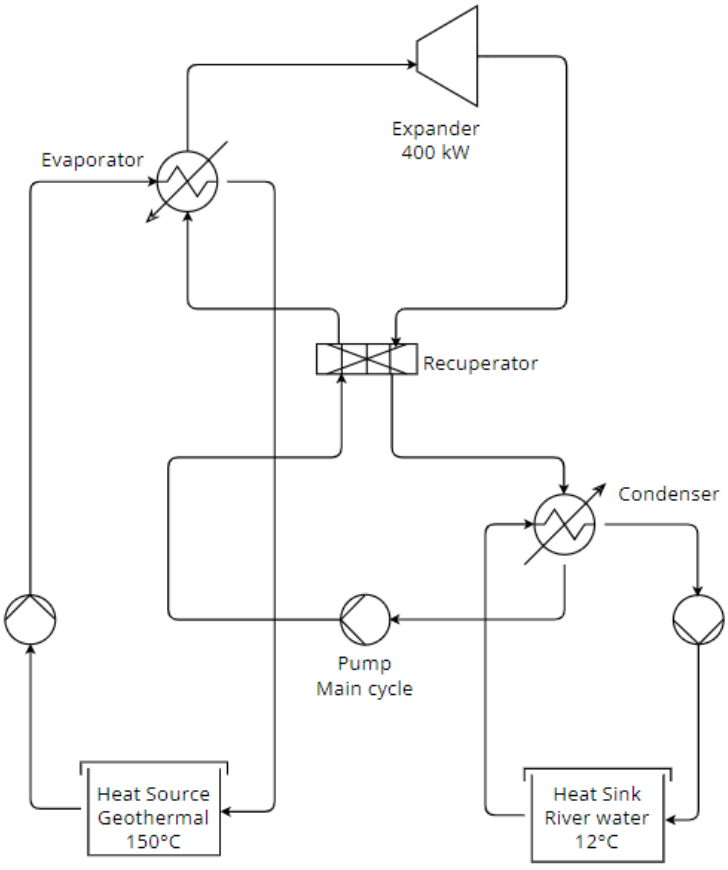

Figure 1: Diagram of geothermal case study

2. Literature Review

2.1. Organic Rankine cycle

The organic Rankine cycle (ORC) is an idealised thermodynamical cycle derived from the Rankine cycle. The Rankine cycle is not discussed in great detail in the literature review. However, appendix A provides a clear overview on the Rankine cycle and on other key thermodynamic concepts such as heat engine and second-law efficiency analysis. The objectives of both cycles are the same. They both convert heat into mechanical work. However, the main difference lies in its working fluid and the temperature range of the application's thermal reservoirs (Ennio & Astolfi, 2016).

2.1.1. Idealised thermodynamic cycle

The idealised organic Rankine cycle uses an organic compound (e.g. a refrigerant or hydrocarbon) to transfer heat and carry out mechanical work. In this idealized cycle, there are four main stages. First, the organic working fluid is evaporated from a liquid form to a gas by adding heat from the hot thermal reservoir to the system. Second, the organic gaseous fluid is allowed to expand. From this expansion, mechanical work is extracted. Third, the organic gaseous fluid is condensed back to a liquid, giving off heat to the cold reservoir or to the recuperator. Fourth, liquid is pressurized using a pump. After these four steps, the working fluid reaches its initial state and the cycle repeats itself (Quoilin S. , 2008).

The different stages of the cycle are shown chronologically in figures 2 & 3. Considering an idealised organic Rankine cycle, the different stages are characterized in the following manner (Quoilin S. , 2008):

- 1 – 2 : isentropic pressurisation of organic liquid
- 2 – 2a : isobaric pre-heating of organic liquid with recuperator
- 2a – 2b: isobaric pre-heating of organic liquid with evaporator
- 2b – 2c : isobaric evaporation of organic liquid with evaporator
- 2c – 3 : isobaric superheating of organic liquid with evaporator
- 3 – 4 : isentropic expansion of organic gas
- 4 – 4a : isobaric de-super-heating of organic gas with recuperator
- 4a – 1 : isobaric condensation with condenser

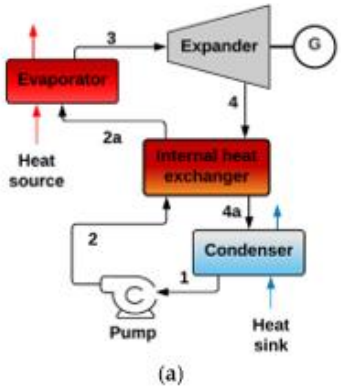

Figure 2: ORC schematic (Jiménez-García, Ruiz, Pacheco-Reyes, & Rivera, 2023)

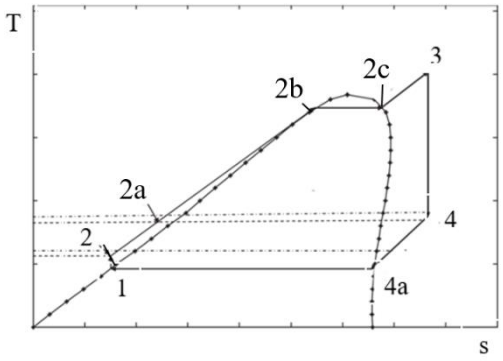

Figure 3: ORC T-s diagram (Roy, Mishra, & Misra, 2011)

The cycle presented in figures 2 & 3 has five main components. These components are: the pump (1-2), the evaporator (2a-3), the expander (3-4), the recuperator (2-2a & 4-4a) and the condenser (4a-1). The recuperator is already an improvement on the standard ORC. However, they are almost always used. (The different components are examined further in chapter 2.5. of the paper). The chosen organic compound working fluid used in ORC has a differently shaped saturated vapour line relative to the Rankine cycle (see appendix A), resulting in a different thermodynamical behaviour of the cycle. Furthermore, this also impacts the lay-out and application of the cycle (Quoilin S. , 2011). All these differences, as well as the design consequences, are discussed further in chapter 2.2.

2.1.2. Comparisson Rankine cycle – organic Rankine cycle

The ordinary Rankine cycle and the organic Rankine cycle have some clear distinguishing properties. The most important difference is the temperature range at which the cycles operate. The Rankine cycle requires a much higher temperature heat source relative to the heat source of an ORC. The ordinary Rankine cycle usually operates at about 400-550 °C (Ibrahim, 2018) whereas an ORC is able to operate from 80°C up to about 330°C (Quoilin S. , 2011).

A key reason why this difference in operating temperatures exist is the working fluid. In order to successfully complete a Rankine cycle, whether it is organic or not, the working fluid must be heated sufficiently in order for the expansion in the turbine to be possible. When gas expands in the turbine, its entropy increases and its temperature decreases as mechanical energy is extracted. If the gas expands beyond the saturated vapour curve of the fluid, small liquid droplets are formed. These droplets will travel at high speed through the turbine and damage its inner structure. Therefore, to avoid the occurrence of these droplets, expansion must be carried out only in the gas state without crossing the saturated vapour curve. Thus the shape and position of this vapour curve is crucial when expanding the fluid in a Rankine cycle. This is shown in figure 4. Organic working fluids tend to have a saturated vapour curve with a vertical or slightly positive slope (also known as isentropic or dry working fluids, respectively), whereas the slope of the saturated vapour curve of water is negative (also known as a wet working fluid). In the Rankine cycle this problem is solved by super-heating the steam. In the ORC, superheating is typically not required because of its vapour curve shape. This allows for lower temperature heat sources to be used (Quoilin S. , 2011) (Ennio & Astolfi, 2016).

In addition, the enthalpy drop of water during expansion is much greater than that of the organic working fluids. A higher enthalpy drop in turn implies a greater mechanical power output of the turbine per cycle. Therefore, ORC's require a much higher mass flow rate to achieve the same power output (Quoilin S. , 2011).

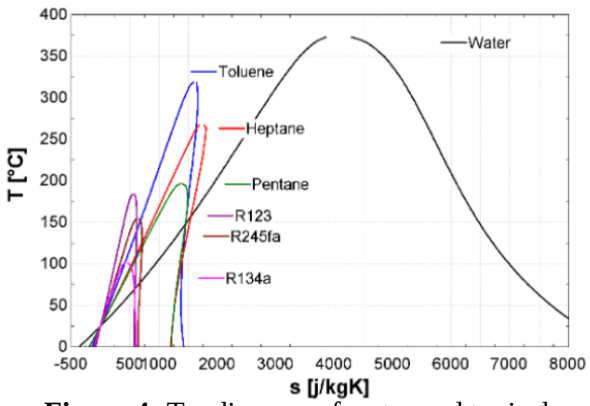

Figure 4: T-s diagram of water and typical organic fluids (Quoilin S. , 2011).

The greater relative mass flow rate of ORC's has an important side-effect, namely, pump power consumption. The power consumption of the pump is proportional to the volumetric flow rate and the pressure head it has to generate. And, because the differences in density between water and the typical organic compounds are not substantial enough, the greater mass flow rate of and ORC also implies greater volumetric flow rate, increasing power consumption. To compare power consumption between both cycles, the back work ratio (BWR) is used. BWR is defined as the pump power consumption divided by the turbine power output. The literature shows that the BWR of a typical steam Rankine cycle is 0.4% whereas an ORC's BWR ranges from 3% up to 10%, depending on the specific organic compound. Thus, pump power consumption plays a much more important role in ORC's compared to water-based Rankine cycles (Ennio & Astolfi, 2016) (Quoilin S. , 2011).

Furthermore, the overall cycle efficiency is significantly different between both cycles. In general, water-based Rankine cycles tend to be more efficient than ORC's. A typical Organic Rankine cycle usually does not exceed an efficiency of 24%, whereas Rankine cycles often have efficiencies well above 30%. The main reason for this difference in efficiency comes from the difference in temperature of the heat source. Higher temperatures of the heat source lead to greater temperature differences between heat source and heat sink, thus leading to greater Carnot efficiencies (Quoilin S. , 2011). Other properties besides temperature are also important in determining cycle efficiency. However, the overall trend between the Rankine cycle and ORC still holds. Rankine cycles are almost always more efficient, but require a higher temperature heat source.

A final key difference discussed is turbine design of both cycles. The turbine of a Rankine cycle allows the gaseous working fluid to expand and extract mechanical energy. In steam Rankine cycles, the pressure and enthalpy drops are very high. To allow for these large drops, several expansion stages are needed. In an ORC, enthalpy drops are much lower, allowing for single-stage or sometimes two-stage turbines to be used, reducing the cost of the turbine substantially. In addition, a lower enthalpy drop across the turbine in ORC's also lower rotational speeds and tip speeds of the blades within the turbine. The lower rotating speeds allow for direct drive of the attached electric generator. The reduced tip speed significantly reduce the stress on turbine blades, reducing their design and production costs (Ennio & Astolfi, 2016) (Quoilin S. , 2011).

Additional considerations on the differences between both cycles can be made, such as the differences in low temperature heat recovery, preheating of working fluids and further superheating specifications. However, these considerations are beyond the scope of this paper. This paper rather focuses in the following chapters on the practical considerations needed for the design and simulation of an ORC.

2.1.3. Real-world behavior of an ORC

The implementation of an organic Rankine cycle in a real-world setting will lead to a deviation of the theoretical maximum efficiency of the cycle. The maximum efficiency is given by Carnot (Dass, 2021). This maximum Carnot efficiency derived from these conditions is reduced by the different irreversibilities present in the system (Ennio & Astolfi, 2016).

In the organic Rankine cycle, there are three main losses in inefficiency because of irreversibilities. Firstly, there are the losses in the pump and expander due to friction and/or leakage of working fluid. Friction causes irreversible heat loss in the system, reducing both mechanical and isentropic efficiency. Leakage of working fluid causes reduction in efficiency by allowing the free expansion of gas, increasing entropy of the system. In addition, losing working fluid increases the cost of supplying new working fluid. Secondly, there are pressure drops in the heat exchangers (condenser, evaporator & recuperator). And thirdly, there are the irreversibilities due to heat transfer with a non-zero temperature difference (Quoilin S. , 2007).

The effect of the different irreversibilities is usually calculated by modelling and simulating organic Rankine cycles and carrying out empirical measurements. However, there also exists a graphical way of comparing the cycle efficiency to Carnot (Bahrami M. , 2020). Such a comparison is shown in figures 5a & 5b. In a T-s diagram the rule of thumb is: the more rectangular the cycle, the closer it is to the ideal Carnot cycle and thus the higher the expected efficiency is. However, a more rectangular T-s diagram also implies a flatter p-v diagram. Therefore, a more efficient cycle is also expected to carry out less work in each cycle. (Quoilin S. , 2007).

A final difference between the ideal and the real-world organic Rankine cycle is that the expansion of the working fluid in the expander is no longer isentropic. Entropy increases in the turbine are due to the free expansion of gas and the friction and pressure drops in the turbine, so the graph shifts to the right. A comparison between an idealised and a real-world ORC is shown in figure 6 (Quoilin S. , 2009).

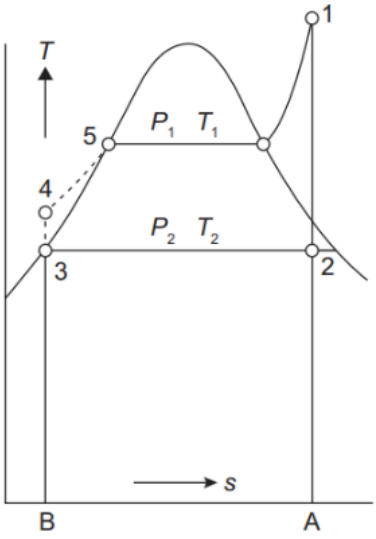

Figure 5a: Ideal organic Rankine cycle in T-s diagram (Ohji & Haraguchi, 2017)

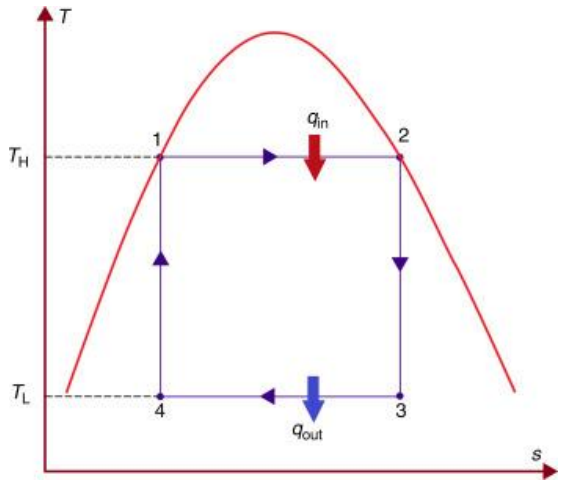

Figure 5b: Ideal Carnot cycle in T-s diagram (Dincer, 2018)

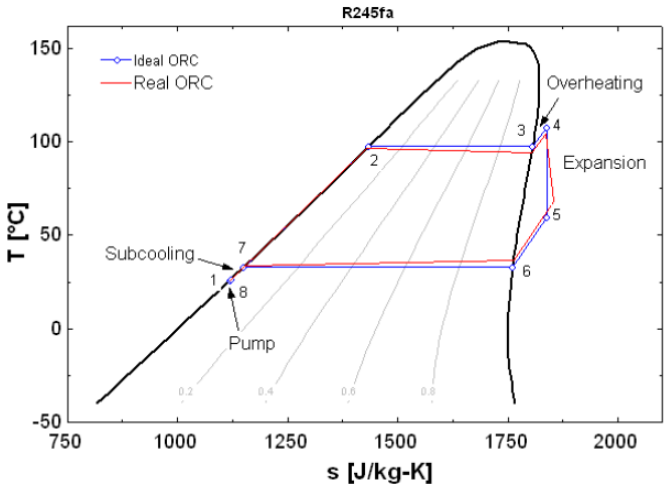

Figure 6: ORC in T-s diagram: ideal/real (Quoilin S. , 2009)

2.2. Working Fluids

Working fluid selection is an essential part in the design process of an ORC. Fluids are mainly selected based on the cycle temperature range, cycle pressure range, thermodynamic and chemical properties and the saturated vapour curve of the fluid. The compatibility of these parameters greatly influences the efficiency of the cycle. Therefore, they are discussed in greater detail in the following paragraphs.

2.2.1. Classifying working fluids by its saturated vapour curve

There are three main types of saturated vapour curves in a Ts-diagram. The first type of fluids are the wet fluids (shown in figure 7a). These working fluids have a saturated vapour curve with a negative slope. Therefore, wet-fluids must be super-heated sufficiently before expansion. Otherwise, expansion would lead to the formation of vapour droplets in the expanding gaseous fluid, damaging the expander. However, often some level of condensation is allowed as long as it does not drop below the minimum dryness fraction at the outlet of the turbine. Typically, this dryness fraction is kept at 85%. Still, most wet fluids require superheating even when considering the dryness fraction. The most common example of a wet-fluid is water, which is used in the ordinary steam-based Rankine cycle (Junjiang & Zhao, 2013) (Ennio & Astolfi, 2016).

The second type of fluids are the dry fluids (figure 7c). Dry fluids have a saturated vapour curve with a positive slope. This positive slope eliminates the problem of condensation which is present in the wet working fluids. The gaseous fluid can expand without the need of super-heating. When the fluid is fully expanded in the turbine, the fluid is still in its gas state. Therefore, an additional heat exchanger (the recuperator) is used to extract heat from the fluid until it reaches its saturated vapour curve. The heat extracted from the gaseous working fluid is recuperated and used to reheat the working fluid in its liquid state. Common examples of dry working fluids are heptane or toluene (Junjiang & Zhao, 2013).

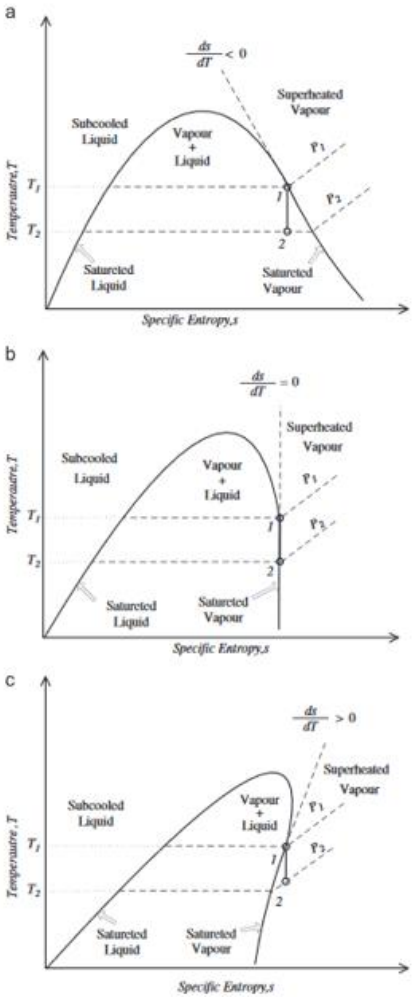

Figure 7: T-s diagrams of the three types of organic working fluids (Junjiang & Zhao, 2013)

The third type of fluids are the isentropic fluids (shown in figure 7b). Isentropic fluids have a (almost) vertical saturated vapour curve. Because of the vertical slope, no super-heating is required and the gaseous working fluid can expand directly without encountering any condensation problems. Typical examples of isentropic working fluids are R123 and R134a (Junjiang & Zhao, 2013).

The dry and isentropic fluids are the fluids most commonly used fluids in ORC. Both fluids do not require super-heating, making them suitable for low-temperature heat source applications where super-heating of fluids may not be possible. However, in theory, the most efficient working fluid in an ORC is a wet fluid with a very steep sloping saturated vapour curve. This is because during any expansion in a turbine the entropy of the expanding fluid increases. If the slope matches the increase in entropy, condensation in condenser can start immediately after the turbine and no additional recuperation heat exchanger is needed. In practice however, fluids with a very steep but wet saturated vapour curve are often not suitable for ORC systems when considering other thermophysical properties. So, isentropic and dry fluids are almost always used in any ORC (Junjiang & Zhao, 2013) (Hung, Shai, & Wang, 1997).

2.2.2. Thermodynamical properties of working fluids

The application and use of working fluids is in a large part dictated by the shape and position of its saturated vapour curve (Junjiang & Zhao, 2013). However, other key chemical and physical properties should be considered when selecting a suitable working fluid. In addition, some of these properties also affect the saturated vapour curve, allowing for further chemical optimisation of working fluids. The most important properties are discussed, however, a full overview of all possible parameters in fluid design is beyond the scope of this paper.

A first key property is the molecular complexity of the working fluid. Molecular complexity is identified by the number of atoms present in one molecule of the fluid. The greater the molecular complexity is, the greater the heat capacity of a compound will be. In the case of the organic compounds used in ORC, the increase of heat capacity is mainly due to an increase in vibrational energy storage potential within the more complex molecules that allow for additional degrees of freedom (Matuszewska, 2020) (Ennio & Astolfi, 2016). Heat capacity of a working fluid is important because of two main reasons. Firstly, greater heat capacity of a fluid allows for smaller temperature drops across the turbine. This is especially relevant for organic Rankine cycles as they operate at lower temperatures. And secondly, greater heat capacity also allows for smaller mass flow in the system, improving the back work ratio of the system (Delgado-Torres, 2018).

A second key property is molecular mass. Molecular mass is defined as the sum of all atomic masses in one molecule of the compound, and plays an important role in the enthalpy drop of the turbine. Greater molecular mass is inversely proportional to the turbine enthalpy drop during expansion. Lower enthalpy of heavier molecule drops in turn are associated with a lower number of stages and lower blade speeds during expansion. This is relevant in ORC design because the molecular mass of the organic compounds are typically 4-10 times greater than water. Furthermore, higher molecular mass compounds typically need larger temperature differences in the heat exchanger, leading to less reversible transfer of heat (Ennio & Astolfi, 2016).

A third important property is the critical temperature of the fluid. The critical temperature is the temperature at which a fluid transforms into a supercritical fluid, a state in which no distinction can be made anymore between liquid and gas phase. The critical temperature also marks the top of the saturated vapour curve in a T-s diagram, making it a key parameter in the positioning of this curve (Xu & Yu, 2014). A first way critical temperature impacts the cycle is through its effect on pressure and volume ratios of expansion. Given a selected evaporation and condensation temperature, a greater critical temperature corresponds with higher pressure and volume ratio's during expansion. This is caused by the exponential relationship of pressure and temperature with the saturation of a fluid. This increase in pressure ratio can be handled by increasing the number of stages of the expander. However, in low power ORC applications a single-stage expander is used. This expander becomes significantly less efficient when pressure ratios become too high, reducing overall cycle efficiency (Ennio & Astolfi, 2016). A second way critical temperature impacts the cycle is through its effect on flow rate. According to Ennio and Astolfi, greater critical temperatures generally correspond with higher volume flow rates (Ennio & Astolfi, 2016).

2.2.3. Environmental and safety considerations

Selecting and optimizing working fluids based on their efficiency in a cycle is a powerful metric. However, additional considerations are necessary to fully evaluate a working fluid. Namely, their environmental costs alongside their safety should be evaluated in the selection process to get a more holistic view.

First, the environmental impact is considered. Working fluids of an ORC can affect the environment by leaking from the system into the atmosphere. Once they are airborne, they will interact with, and therefore also change the composition of, the atmosphere. The specific chemical composition of the working fluid determines the magnitude of the impact. To estimate this impact, Global Warming Potential (GWP) and Ozone Depletion Potential (ODP) are used. GWP is a measure of the relative potency of a greenhouse gas (European Environment Agency, 2023). It measures how much infrared radiation the fluid absorbs over a given period of time (Pedone Bandarra Filho & Heleno Pontes, 2016). ODP is a measure for the relative degradation of the ozone layer caused by a chemical compound (Bahrami, Pourfayaz, & Kasaeian, 2022). According to the new standards, a working fluid must have zero ODP and a GWP lower than 150 (Bahrami, Pourfayaz, & Kasaeian, 2022). For more details on ODP and GWP, see appendix B.a.

Second, the safety of the fluid in its application must also be considered. Safety of working fluids is analysed in using two main parameters: flammability and toxicity (Bahrami, Pourfayaz, & Kasaeian, 2022). Flammability is classified by the ASHRAE Standard 34 and the ISO standard 817. These standards are based on heat during combustion, lower flammability level and laminar burning velocity. Both standards also use a 3-class system to define the flammability of the compound. A class 1 compound shows no flame propagation whereas a class 3 compound exhibits highly flammable behaviour. Most working fluids used in an ORC are either a class 2 or class 3 compound and therefore are almost always considered to be flammable (Linteris, Bell, & Mclinden, 2019). This flammability is important to consider when looking at the overall safety of an ORC installation, especially when they are combined with gas-turbine cycles (Bahrami, Pourfayaz, & Kasaeian, 2022). Toxicity in the context of working fluids and refrigerants is classified using the human toxicity potential (HTP). HTP is an index that reflects the potential harm a single unit of the chemical released into the environment can do (Hertwich, Mateles, Pease, & McKone, 2001) (Bahrami, Pourfayaz, & Kasaeian, 2022). A discussion of other environmental and economic considerations during the selection of working fluids can also be found in appendix B.b. and B.c.

2.2.4. Summary on working fluids

Working fluids in ORC typically have a positive or isentropic saturated vapour curve. This ensures dry expansion. In some cases, the saturated vapour curve has slightly negative slope to compensate for the isentropic efficiency of the turbine. The molecular complexity of the compound mainly influences the heat capacity of the fluid. The molecular mass of the compound mainly influences the enthalpy drop during expansion. A good working fluid should have 0 ODP and a GWP below 150. Other fluid properties such as flammability and toxicity should also be considered.

2.3. Different cycle designs

2.3.1. Sub-and super critical cycle designs

There are two kinds of cycles: the subcritical cycle and the supercritical cycle. The subcritical cycle operates in such a way that the critical temperature and critical pressure of the working fluid are greater than the operating temperatures and pressures within the system. Conversely, the supercritical cycle does reach temperatures and pressure greater than the critical temperature and pressure. The supercritical nature of this cycle offers some significant advantages in thermal efficiency compared to the subcritical one, but also some clear practical disadvantages. To explain these differences, consider the subcritical and supercritical cycles represented in figure 8. In both cycles, the temperature progression of the heat fluid is more or less the same. Its temperature decreases in a linear fashion as it gives off heat (shown by the orange lines). However, the temperature progression of the working fluids does differ (shown by the green cycle lines). A subcritical cycle working fluid's temperature first increases quasi-linearly during preheating, then becomes constant during evaporation and finally increases quasi-linearly again during superheating. A supercritical cycle does not have a constant temperature region as it does not experience a phase transition. It changes instantly from a liquid to a critical fluid. As a consequence of this, the temperature progression of the heat source fluid and that of the working fluid are much more aligned in the supercritical cycle. If further optimized, both curves can be made to match almost exactly, reducing the average temperature difference at which heat is exchanged. Therefore, less entropy is generated in the system due to heat transfer between both fluids. Less entropy creation results in the higher thermal efficiency of the system (Ennio & Astolfi, 2016).

Despite the clear advantage of the supercritical cycle in terms of thermal efficiency, there are also clear disadvantages. Namely, to have a working fluid achieve its critical state, high pressures or temperatures are needed. In ORC applications, high temperatures are not available so high pressure must be achieved. These high pressures are only achievable by large and expensive multistage centrifugal pumps which consume much more power. In addition, the heat exchanger used in the cycle must be built to withstand the high operating pressure, increasing its costs drastically (Ennio & Astolfi, 2016). Because of these reasons, supercritical cycles are only chosen over subcritical ones in specific applications where the benefits outweighs its costs (Ennio & Astolfi, 2016).

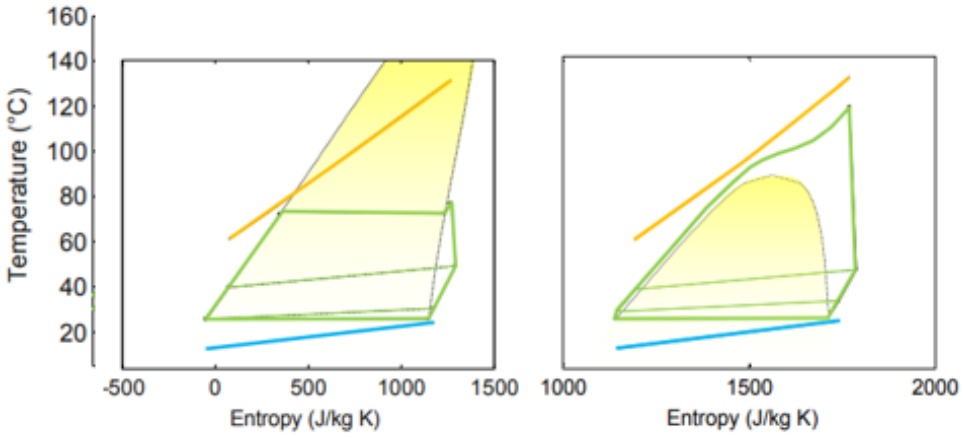

Figure 8: T-s diagrams of subcritical (left) and supercritical (right) cycles (Ennio & Astolfi, 2016).

2.3.2. Multi-pressure level cycle designs

Previously discussed cycles are all single-pressure level cycles. In these cycles, evaporation happens only at one pressure. However, other cycle designs do exist. For example, multi-pressure level cycles. In these cycles evaporation is carried out in different steps, with each step having a different evaporation pressure. The goal of this cycle is similar to that of the supercritical cycle in the single-pressure level cycle, improve the efficiency of the heat transfer in the cycle. This is done by matching the temperature progression of the heat source's fluid to that of the cycle's working fluid such that the temperature difference at which heat is exchanged is minimized. An example of a multi-pressure level cycle design is shown in figure 9 (Ennio & Astolfi, 2016) (Manente, Lazzaretto, & Bonamico, 2017).

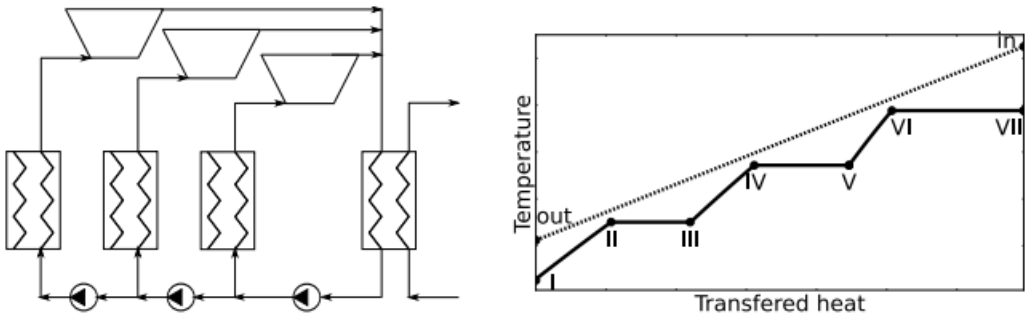

Figure 9: T-s diagram of a multi-pressure level cycle (Walraven, Laenen, & D'haeseleer, 2012).

2.5. Analysis of main components

2.5.1. Expander

2.5.1.1. General overview

There are three main types of expanders: volumetric expanders, radial turbines and axial turbines. As the desired net output of the turbine in the analysis of the geothermal ORC of this paper should be around 400 kW, the expander selected is a radial inflow turbine.

Radial inflow turbines are essentially the same as radial centrifugal compressors, but with reverse flow and angular velocity. Accordingly, the flow enters the turbine through the volute and is guided by inlet guide vanes into the rotor. As a result, the fluid has considerable angular momentum before it reaches the rotor. As the fluid passes through the rotor, the rotor utilises this angular momentum to produce power. The fluid then flows through a diffuser to convert some fluid kinetic energy into static pressure to improve efficiency. In comparison to an axial turbine, the radial turbine can handle higher pressure ratios per stage, and is also smaller in size. Another advantage are the inlet guide vanes, which are sometimes variable, and ensure a higher efficiency in off-design conditions. Radial inflow turbines are generally used in the range 50 – 500 kW. (Pettinato, Rainer, & Leonid, 2022)

2.5.1.2 Thermodynamics of a radial inflow turbine

First, the efficiency of the turbine is considered. One of the most powerful tools to calculate the efficiency is via the entropy production method. Entropy production (the rate at which entropy increases) is a measure of how close a process approaches reversibility. The closer to reversibility, the more efficient a process. Thus, it is clear that during the design of a turbine, entropy production must be minimised in order to achieve maximum efficiency.

Entropy production occurs due to the summation of four distinct contributions which stem from the products of flows and forces. These contributors of entropy production are heat transfer, mass transfer, viscous dissipation and chemical reactions. (Demirel & Gerbaud, 2019) However, in the actual turbine, the entropy production is almost exclusively caused by viscous dissipation and turbulent dissipation on account of velocity fluctuations. Viscous dissipation is typically the primary mechanism for dissipating turbulent kinetic energy. The turbulence can also contribute to the main flow, albeit as a minor factor. Therefore, the viscous dissipation component and overall dissipation tend to align closely (Wang Z. , 2023).

To predict entropy production inside a turbine, advanced kinetic and statistical models are needed. However, these models necessitate more extensive data than what is often readily available to describe non-equilibrium systems. Therefore, a more phenomenological approach is needed. In this approach, models are based on the Gibbs equation, which combines the first and second law of thermodynamics, and the balance equations. In these calculations, the Gibbs equation[1] plays a pivotal role by dictating the rate of entropy production. Once the entropy production is known, the loss of energy can be easily calculated via a simple formula[2]. However, even when these more simple models are used, entropy production is still almost impossible to calculate without advanced computational fluid dynamics. Therefore, to determine entropy production in this paper, references from previous academic work are used.

In previous academic work, similar ORC configurations to this paper have found isentropic efficiencies ranging from 0.87 - 0.92 (Chen, Liu, & Liu, 2021), (Feng, Li, & Huang, 2023), (Wang, Zhang, & Xia, 2019), (Sauret & Petrie-Repar, 2012), (Noughabi & Sammak, 2018) and (Sauret & Gu, 2014). The most similar study to this paper is from Marcuccilli and Mathiasin, where they found an efficiency of 0.88 for expanding isobutane from 35 bar at 153°C to 3.62 bar (Marcuccilli & Mathiasin, 2006). This paper will thus use an isentropic efficiency of 0.88 in further calculations.

2.5.2. Heat exchangers

2.5.2.1. General overview

There are three main ways the flows within a heat exchanger are executed. First, parallel-flow, in which the hot and cold fluids follow the same direction. Second, counter-flow, in which the hot and cold fluids have an opposite direction. And third, cross-flow, where the hot and cold fluids flow perpendicular to each other.

In general, counter-flow heat exchangers outperform parallel-flow and cross-flow heat exchanger when one considers the amount of heat that is exchanged for a given surface area and temperature difference. This is because of the more uniform temperature difference throughout the heat exchanger between the hot and cold flow. If one fluid's temperature is kept at constant temperature (e.g. during isobaric condensation or evaporation) the difference between the two configurations is minimal. However, in most power cycles, there is some need of preheating, superheating and de-superheating. Therefore, counter-flow heat exchanger are usually preferred (Rops, Hossain, & Boerboom, 2021). However, other types of flow heat exchangers still serve a purpose. In Parallel flow heat exchangers hot and cold flow temperatures converge during the transfer of heat, leading to less efficient heat transfer but potentially beneficial effects on the applicability of the fluids. (Enerquip, 2018). For example, when there is a high risk of freezing of one of the fluids after the heat exchanger, the limited heat exchange of parallel flow may be beneficial (Brazetek, 2012). Cross flow is considered to be a compromise between parallel and counter flow. The effectiveness of a cross flow heat exchanger is lower than that of a counter flow heat exchanger, however the flow area required for cross

[1] Gibbs energy equation: $G = U + pV - TS = H - TS$ (Dass, 2021)

[2] Energy loss equation: $\dot{E}_{loss} = T_0 \,.\dot{S}_{prod}$ with $\dot{S}_{prod} = \frac{dS}{dt} = \int \sigma dV$ (Demirel & Gerbaud, 2019)

flow is smaller. Cross flow heat exchangers also are generally speaking easier to produce compared to parallel and counter flow heat exchanger, which drives down the investment costs (Linquip Team, 2023).

Cross flow is typically achieved in a shell and tube heat exchanger (S&THX). A shell and tube type heat exchanger is essentially a bundle of parallel tubes in a cylindrical shell. Baffles are commonly placed in the drum to increase the residence time and turbulence of the fluid on the hull side, which increases the heat transfer coefficient U. In ORC power systems, shell and tube heat exchangers are preferred for the different heat exchangers. Only the Recuperator typically has a counterflow plate heat exchanger design. To summarise, the general preference for S&HTX's comes from its following characteristics (Sacome, 2019):

- High operating pressures (able to withstand high pressure of a typical power cycle)
- High operating temperature (able to withstand high temperatures of a typical power cycle)
- Easy inspection
- Easy to enlarge for future expansion
- Lower installation costs

These equations that describe heat transfer with a heat exchanger are:

(1) The equations for total heat transfer between the hot and cold fluids (Van de Paer, 2022):

$$\dot{Q} = \dot{m}_{hot} \,.\, \left(h_{hout,in} - h_{hout,out}\right) \dot{=} \dot{m}_{cold} \,.\, \left(h_{cold,in} - h_{cold,out}\right)$$

(2) The equations for heat power of the heat exchanger using the LMTD method (Van de Paer, 2022):

$$\dot{Q} = \mathrm{U} \,.\, \mathrm{A} \,.\, \overline{\Delta T} \qquad \& \qquad \overline{\Delta T} = \frac{\left(T_{h,in} - T_{c,out}\right) - \left(T_{h,out} - T_{c,in}\right)}{\ln \frac{\left(T_{h,in} - T_{c,out}\right)}{\left(T_{h,out} - T_{c,in}\right)}} \qquad \& \qquad \overline{\Delta T} = F * \overline{\Delta T}_{Shell-Tube}$$

(3) The equations for heat power of the heat exchanger using the ε-NTU method (Van de Paer, 2022):

$$\dot{Q} = \varepsilon \,.\, C_{min} \,.\left(T_{h,in} - T_{c,out}\right) \qquad \& \qquad \varepsilon = \mathrm{f}\left(\mathrm{NTU}, \frac{C_{min}}{C_{max}}\right) = \frac{\dot{Q}}{\dot{Q}_{max}} \qquad \& \qquad NTU = \frac{UA}{C_{min}}$$

The first set of equations (1) are used in the modelling of an ORC to determine the required amount of heat transfer between both fluids. The second and third set of equations (2)/(3) are used to size the heat exchanger according to the required amount of heat of the cycle. The LMTD method is used when the in-and outlet temperatures of the hot and cold fluids of the heat exchanger are known. The ε-NTU method is used when only the inlet temperatures of the hot and cold fluids are known (Roetzel, Luo, & Chen, 2019) (Ennio & Astolfi, 2016). In this paper, a geothermal ORC is modelled in which the in-and outlet temperatures of the different heat exchangers are known. Therefore, the LMTD-method is used to size the heat exchangers (Primo, 2020). A heat exchanger is sized by determining the necessary UA-value for a given amount of necessary transferred heat.

2.5.2.2. Fouling factor and cross flow correction factor

In order to size a heat exchanger in an adequate manner, different correction factors must be considered. In this paper, two key correction factors are discussed, namely: the fouling factor and the cross flow correction factor. The fouling factor is a measure for the reduction of the UA value over time due to fouling deposits in the tubes of the heat exchanger. This sediment that is left on the inside of the tubing increases thermal resistance, therefore reducing the UA value of the heat exchanger. The most common types of fouling are chemical fouling (chemical reactions with the tubing), biological fouling (growth of organism), deposition

fouling (settling of particles on the surface) and corrosion fouling (an additional insulating corrosion layer). Fouling can be partially prevented by for example using corrugated tubes. These tubes especially reduce deposition and chemical fouling. Deposition fouling is reduced by the greater level of turbulence that is generated at lower speeds due to the corrugated tubes. Chemical fouling is reduced because of the reduced temperature difference between the fluid temperature and the tubing wall temperature (HRS, 2024). Fouling can be partially reverted by ensuring good maintenance of heat exchangers and by cleaning the tubes, shells and plates on a regular basis.

The cross flow correction factor F is a correction factor used to account for the differences in heat transmissibility between cross and counter flow (Kumar, Bhatti, Krishna, Vundru, & Neelapu, 2006). Because, the exchanged heat for a given temperature difference is always greater for counter flow relative to cross flow. This correction factor F lies between 0 and 1 and is used in the LMTD method to adjust the established $\overline{\Delta T}$ (see equations (2) of section 1.5.2.1.). The correction factor F depends on the in-and outlet temperatures and on the construction of the shell and tube heat exchanger. In this paper, a shell and tube heat exchanger is used with a one-shell pass and an even number of tube passes. This correction factor is derived from charts by using the parameters R (the capacity ratio) and P (measure of heat exchanger effectiveness) as can be seen in the following equations and in the associated figure 10:

$$R = \frac{T_1 - T_2}{t_2 - t_1} \quad \& \quad P = \frac{t_2 - t_1}{T_1 - t_1} \quad \& \quad \overline{\Delta T} = F * \overline{\Delta T}_{Shell-Tube}$$

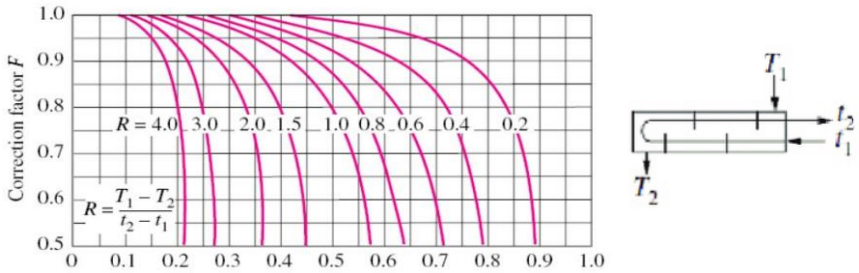

Figure 10: One-shell pass and even number of tube passes (Nimish Shah, 2014)

2.5.2.3. Exergy destruction in heat exchangers

The basic working principle of any heat exchanger is quite straightforward. A heat exchanger transfers energy in the form of heat from one fluid to another using conduction. This heat conduction is driven by a difference in temperature between both fluids, and heat energy flows from the hot fluid to the cold fluid. However, any transfer of heat with a non-zero temperature difference will inevitably lead to an increase in entropy, reducing the sum of exergy of both fluids when they have exited the heat exchanger. The exergy of a system is a measure of the quality of energy and is defined as the maximum work a system can output. So, exchanging heat at a non-zero temperature difference reduces the total ability to do work of both fluid flows of the heat exchanger. This exergy analysis is a common tool to optimize designs of a power cycle and any of its components, including the heat exchangers (Jaffe & Taylor, 2018).

In general, there are three main sources of entropy increasing, factors in heat exchangers (Mehdizadeh-Fard, Pourfayaz, & Maleki, 2021):

- Heat transfer at a non-zero temperature difference from the hot to the cold stream
- Pressure losses because of friction in the heat exchanger (discussed in chapter 2.5.2.4.)
- Emission of heat energy to its surroundings (not discussed in this paper).

By far the most important exergy destroying factor in the heat exchanger is non-zero temperature difference. Therefore, to minimize the amount of exergy destruction, heat must be transferred across the smallest possible temperature difference. This implies that the heat exchanger must have a very large surface area and/or a very large heat transmissibility coefficient. Also, the temperature distribution of both hot and cold flows must be optimized such that they match as close as possible (see chapter 2.3. Different Cycle Designs). The reduction in heat transfer irreversibilities can lead to significant increases in the overall thermal efficiency of a power plant such as a geothermal ORC power plant, which is discussed in the methodology section of this paper (Mehdizadeh-Fard, Pourfayaz, & Maleki, 2021).

2.5.2.4. The pinch point

The pinch point is an essential parameter of any heat exchanger. This point in the heat exchanger is the point where there is the smallest temperature difference between the hot and cold flows. For example, consider the evaporator of a subcritical ORC. When the working fluid passes through the evaporator, heat is added to the fluid by the heat source. As a consequence of this, the temperature of the heat source fluid decreases in a quasi-linear fashion. Also, the temperature of the working fluid increases at first and then remains constant during the phase transition from liquid to gas state. This process is shown in figure 11 for any given evaporator. In this figure, the heat source fluid flows from right to left and the working fluid flows from left to right. It shows that the pinch point location depends on the different temperature curves of the hot and cold flows (Dimain, Bildea, & Kiss, 2014).

Pinch point location and its ΔT are essential parameters as the heat transfer between the hot and cold streams are most constrained here. The ΔT at this point in the heat transfer must remain positive, i.e. the hot stream must remain at higher temperature than the cold stream. If this is not the case, heat will flow back from the cold stream to the hot stream, disrupt the working of the heat exchanger and drastically reduce the heat exchanger's effectiveness. Furthermore, in the case of an ORC, the working fluid will more than likely not be fully evaporated or condensed, leading to problems in the turbine and the pump. Because of these reasons, the pinch point is a key parameter when designing temperature regimes and choosing working fluids. Usually a positive temperature difference of at least a few degrees K is maintained during design, to ensure no negative ΔT is created. (Dimain, Bildea, & Kiss, 2014) (Ye, Xu, Chen, & Wei Guang, 2020).

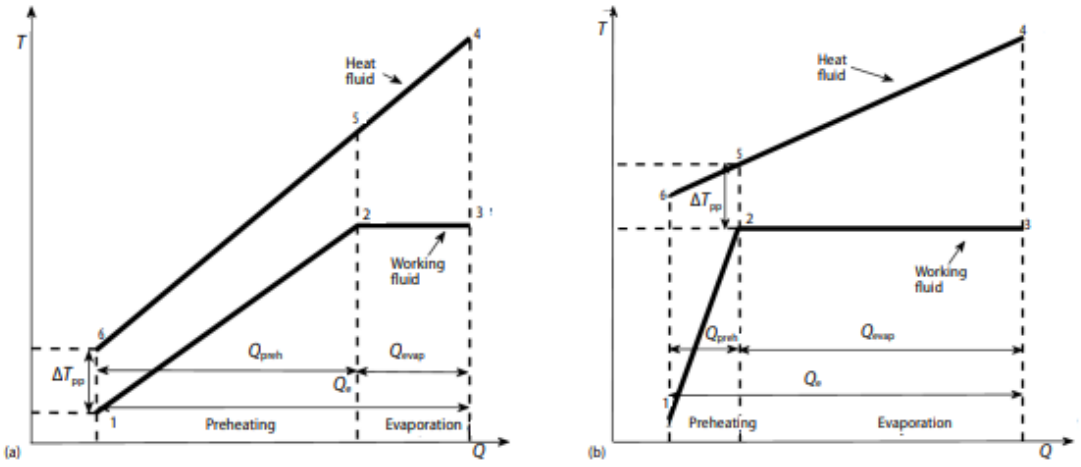

Figure 11: Pinch point comparison (Ye, Xu, Chen, & Wei Guang, 2020)

2.5.2.5. Pressure drops in a shell and tube heat exchanger

One of the efficiency losses present in a heat exchanger are the pressure drops across it. As is shown in section 2.5.2.3, pressure drops lead to exergy destruction in heat exchanger just as temperature difference during heat transfer, albeit to a lesser extent. Still, it is important to recognize these losses and evaluate them in the discussed application. In the ORC of this paper, a shell and tube heat exchanger is used. Therefore, when discussing pressure losses in a S&THX, a distinction needs to be made between pressure losses on the shell side and on the tube side. The tube side pressure drops are not discussed in the literature review. This is because the working fluid in a geothermal application typically flows through the shell and the heat source fluid flows through the tubing. And, because only the working fluid side of the cycle is discussed in the paper's analysis, tube side pressure drops are not discussed further. Furthermore, an additional distinction needs to be made depending on the phase state of the fluid. The single-phase pressure drop approach is used when the working fluid is its pure liquid or gas form, e.g. in the recuperator or in the superheater. The two-phase pressure drop approach is used when the working fluid is transitioning between two phases, e.g. in the evaporator or in the condenser (Nuclear Power, 2024). This presence of a second phase makes the calculation of pressure drops considerably more difficult.

There are two main methods to calculate the single-phase shell side pressure drops in shell and tube heat exchangers (Lara-Montaño, Gómez-Castro, & Gutiérrez-Antonio, 2020). First, there is the Kern method. This method is easier to use than the second method, but is somewhat less accurate and less applicable to specific cases. In the Kern method, the shell-side pressure drop is given by the following equation:

$$\Delta p_{shell-single-phase} = \frac{\rho_s v_s^2}{2} * \frac{L}{B} * \frac{D_s}{D_e} * f_s$$

With
v_s = shell-side fluid velocity
f_s = shell-side friction factor
ρ_s = shell-side fluid density at mean temperature
D_s = shell diameter
D_e = equivalent shell diameter
B = Baffles spacing
L = tube length

And second, there is the Bell-Delaware's method. This method covers a much wider range of shell and tube heat exchangers, considering a wider range of parameters. The calculation of pressure drops has three main components instead of just one. Pressure drops are calculated in central section, in the window section and in the in-outlet section of the shell and tube heat exchanger separately, and then combined into a single pressure drop across the entire heat exchanger. However, the determination of these pressure drops is much more tedious and complex then the Kern method (Saari, 2010) (Lara-Montaño, Gómez-Castro, & Gutiérrez-Antonio, 2020). Furthermore, the overall size of the pressure drop losses is expected to be small relative to other losses in the cycle. Therefore, the kern method is the preferred option for the analysis of this paper, as the reduced accuracy of Kern relative to Bell-Delaware is not expected to impact the results in a meaningful way.

2.5.3. Pump

Another main component is the pump. It is of great importance to have an efficient pump. Since the back work ratio of the organic cycle is higher than the steam cycle, the pump must deliver more relative work.

The most commonly used pump in organic Rankine cycles is the centrifugal pump. They are easily maintained, have a relatively high efficiency and are simple to construct. Furthermore, They deliver a

continuous, pulsation-free current. (Klimaszewski & Klonowicz, 2020) As an added bonus, there is a satisfying symmetry that the pump and the turbine are essentially the same 'machine'. Since the pump is quite similar to the turbine, its working principles are not discussed in great detail.

A centrifugal pump is composed of a impeller (rotor) followed by a diffuser. As the fluid flows through the impeller, its angular momentum increases. This kinetic energy from the angular momentum is then converted into pressure energy by the diffuser. (Hall & Dixon, 2013)

The theoretical and manometric pressures are respectively:

$$p_E = \rho \,.\, u_2 \,.\, c_{2u} \qquad\qquad p_{man} = p_E \,.\, k \,.\, \eta_{hydr.}$$

With u_2 being the peripheral velocity at the outer diameter of the impeller, and c_{2u} is the projection of c_2 (the absolute velocity of the fluid) onto u_2. Furthermore, k is a factor that takes into account the non-ideal flow due to the limited number of blades, and η_{hydr} takes into account the internal pressure losses within the pump (Janssen, 2022). The pump should be sized so that its operating point is at (or very close to) its best efficiency point (BEP); at this flow rate, the pump delivers optimal performance.

In most ORC configurations, the turbine and pump are independent from each other. Larjola, a Finnish engineer, figured it would be more efficient to put the turbine and pump in direct drive. So as to limit drivetrain and other losses, and to have a more compact system (Larjola, 1995). Some ORC manufacturers, like Triogen, offer this configuration (Triogen, 2024).

2.5.4. Piping system

The pipes are an essential part of any ORC installation. It connects the different main system components of the cycle. There are two kinds of losses in the piping: heat loss and friction loss. As the piping carries fluid of up to 150 °C, they should be insulated, thereby reducing the heat loss to the environment. Heat loss to the environment is given by the following equation (Van de Paer, 2022):

$$\dot{Q} = L \,.\, \frac{(T_1 - T_2)}{R_{per\ meter}} \qquad\qquad R_{per\ meter} = \frac{1}{2\pi r_1 h_1} + \frac{\ln\frac{r_2}{r_1}}{2\pi\lambda_{12}} + \frac{\ln\frac{r_3}{r_2}}{2\pi\lambda_{23}} + \frac{1}{2\pi r_3 h_3}$$

To calculate the head loss in the piping, the following equations based on Bernoulli's law and the derived equations of Darcy-Weisbach are used:

$$\Delta P = \rho g h_f \qquad\qquad h_f = \sum_i K_i \,.\, \frac{u_i^2}{2g}$$

With orifices K_i (diameter changes, curves, valves). And the resistance coefficient K of a straight pipe $K_{straight\ pipe} = f \,.\, \frac{L}{d_h}$. With f the drag coefficient, L the length of the pipe and d_h the hydraulic diameter (Hereijgers, 2021).

These different formulas allow for the analytic determination of friction loss and heat loss. However, empirical measurements of real-world ORC systems are also often employed when determining these losses (Yan, Yang, Yang, Zhang, & Guo, 2020).

2.6. Geothermal energy

2.6.1. Geothermal heat generation

Geothermal energy is energy stored beneath the surface in the form of heat. This heat is present in the earth because of four main reasons. The first reason why the earth carries some amount of heat comes from the formation of the planet itself. As it takes a long time for heat to dissipate into space, a significant part of the primordial heat from the creation of the earth is still present today. Furthermore, other later events such as the impact of a Mars-sized object with earth resulting in the creation of the moon, added to this primordial storage of heat. The second reason is frictional heating, caused by denser materials sinking to the centre of the earth. The earth's gravity exerts large compression forces towards the centre of the earth, generating friction due to the contraction of earth layers. This results in additional heat. The third reason is the decay of radioactive isotopes. The earth's crust and mantel is filled with radioactive elements such as potassium uranium and thorium. When these instable isotopes fall apart, heat is generated as the decomposition of these isotopes are all exothermic. The final reason why the earth has significant heat available is the combination of high pressures and several physicochemical exothermic reactions. These processes typically take place in the earth's mantle. Given the high pressures and high temperatures of the mantle, instable minerals are formed and change phase continuously. These changes of phase generate heat (Williams, 1997) (ICGC, 2011). All the above mentioned heat source are responsible for an increased temperature of the earth. The average temperature of the earth at the surface is about 15°C and increases when moving towards the earth's core, reaching about 5000°C at its centre. It is this trapped heat that can be used in geothermal energy extraction.

2.6.2. Geothermal heat sources

In general, there are four main types of heat sources in geothermal energy engineering. First, there are the hydrothermal reservoirs. These reservoirs contain hot brine, water or steam that is trapped in porous rock formations, typically found at depths ranging from 0.5 to 2. km. These fluids are extracted and serve as the heat source of an ORC power cycle, with the temperature ranging from 90-200°C (depending on the given circumstances) (Dambly & Lyman, 1982). Second, there are the geopressured reservoirs. These reservoirs also contain high temperature brine, water or steam, and are also trapped in a permeable rock layer but are found much deeper underground. Therefore they are exposed to much higher pressures and have a high concentration of mineral, salts and dissolved gasses. These additional by-products can be filtered out and often serve as supplementary revenue for the power plant when using geo-pressurized reservoirs (Butterfield, Gillette, & Shin, 2014). The temperature of these fluids is often somewhat higher compared to those of thermal reservoirs, ranging from 150 - 330 °C. However, deeper drilling is needed, with depths ranging from 2-3 km typically (Scott & Alderton, 2021). Third, there are the hot dry rock reservoirs. These are rock formations in which no liquid is readily available to pump to the surface and extract the heat from. Instead, the rock must be fractured and a fluid circulation must be established by pumping water from the surface through the underground rock formation. The hot rock formations conduct heat to the water and this heat is then extracted when the water is pumped back up to the surface (Butterfield, Gillette, & Shin, 2014). Typical depths for these dry rock formations range from about 1 to 3 km, and the water that is pumped to the surface its temperature ranges from 150 – 200 °C (Loewer & Keim, 2022). And finally, there are the magma reservoir heat sources. These magma reservoirs are found much deeper in the earth and have a much greater temperature than the other sources of geothermal energy. They are found at depths ranging from 3 to 10 km deep and the temperature ranges from 700 – 1200 °C (Butterfield, Gillette, & Shin, 2014).

The first three sources of geothermal heat are of interest for this paper, namely: hydrothermal reservoirs, geo-pressurized reservoirs and dry rock reservoirs. They exhibit temperature ranges that fall within the

operating range of an ORC cycle. The magma reservoirs offer a heat source temperature that is too great to be used effectively in an ORC. Other power cycles such as the Rankine cycle are more suitable in this case.

Another way of categorizing geothermal energy is by its extraction process. In geothermal energy, there are two main extraction concepts: hydrothermal systems and petrothermal systems. Hydrothermal systems utilise hot water from deep aquifers as a heat source. This system makes use of two wells, one for pumping up the hot water, and the other for the cooled water to be put back. It is clear that the wells must be sufficiently distanced from each other, so as to not affect the temperature of the hot water (used geothermal reservoirs and geo-pressurized reservoirs). Petrothermal systems on the other hand, do not have a need for aquifers. Instead, only the temperature at depth is of importance. Then, water is pumped down into the hot rock, and subsequently pumped back up again, with the hot rock serving as a heat exchanger (used for hot dry rock reservoirs and magma reservoirs) (Agemar, Weber, & Schulz, 2014).

2.6.3. Geothermal power generation

One of the clear advantages of geothermal energy applications is its relatively low CO2 emissions. Considering the global average, for every kWh of electric energy generated by geothermal power about 122g of CO2 are emitted. However, the range of CO2 emissions between different power plants is substantial, varying from 4 up to 740 g/kWh. Still, on average, geothermal power plants emit substantially less CO2 relative to natural gas, oil and coal emissions (Ármannsson, 2003). Furthermore, modern geothermal plant installations typically have their CO2 emissions below 100g/kWh. Another advantage of geothermal power is its constant power source. Contrary to some other sustainable emission of below low-carbon power supplies such as solar or wind, geothermal heat can be extracted at a near constant rate, making geothermal power more predictable and better applicable. Still some clear disadvantages of geothermal must also be recognised. Geothermal power requires deep drilling operations which can disturb earth layers and cause small earthquakes, especially when dealing with hot dry rock reservoirs (Khansefid, Yadollahi, Müller, & Taddei, 2022). Furthermore, geothermal heat extraction can cause temperature drops of the surrounding area at the earth's crust, impacting nearby households and ecosystems (Kagel, Bates, & Gawell, 2005).

Geothermal energy installations have a large range in potential power outputs. Depending on the size of the power system, the used heat source type and heat source temperature, electrical power output of the installation ranges from a few hundred kW up to 40MW (Tomarov & Shipkov, 2017).

Geothermal energy is an excellent energy source for the ORC due to a very high capacity factor, low operating temperature and good predictability and reliability. Geothermal energy is also used for other purposes, such as: district heating, industrial processes and desalination (Fridleifsson, 2008). In the methodological analysis of this paper, a geothermal hot dry rock reservoir of 150°C is used to analyse a small scale ORC with an output of 400kW in mechanical power.

Some of the other possible energy sources used in ORC are discussed in appendix C.

3. Methodology

3.1. Overview

An ORC is modelled with a heat source of 150°C, heat source mass flow rate of 10 kg/s and a heat sink of 12°C. The main characteristics of the cycle's components can be found in table 1.The model is built in different steps, each step expanding on the previous model iteration. Cycle efficiencies are compared across model iterations and working fluids. Heat exchanger sizing relative to cycle efficiency is also examined. A sensitivity analysis is carried out on the final model iteration.

Table 1: Main cycle components' characteristics

Component	Characteristics
Evaporator	• 3 sections: preheating, evaporation & superheating • Shell and tube heat exchanger • Cross flow • Stainless steel
Recuperator	• Copper plate heat exchanger • Counter flow • Copper
Condenser	• Shell and tube heat exchanger • Cross flow • Stainless steel
Expander	• Radial inflow • Power of 400 kW • Isentropic efficiency of 0.88
Pump	• Pressure head of 27 bar • Power of 26 kW • Efficiency of 0.8
Piping	• 5m of stainless steel pipes with diameter of 350 mm • 5m of stainless steel pipes with diameter of 125 mm • 4 appendages of 90° present • Insulated with 15cm of PIR insulation

3.2. Simulation tools

To model and simulate the geothermal ORC of the case study, Python is used. This is because it is an open source language and has an extended range of useful libraries. One of these libraries is the CoolProp database. CoolProp offers extensive information on the thermodynamical properties of different organic compounds that are needed (CoolProp, 2023). Python is preferred over other simulating tools such as EES or Matlab because of the availability of these libraries and because of the freedom it provides.

3.3. Model

3.3.1. Baseline model

To evaluate thermodynamic state of any compound, two state variables must be defined. All the other possible state variables are then determined by this pair of variables. To build the first baseline model, five key cycle states are identified, based on the parameters of the case study. These cycle states are: evaporator outlet/turbine inlet, turbine outlet, condenser inlet, condenser outlet/pump inlet, pump outlet/evaporator inlet. First, the turbine inlet state is determined by the evaporating pressure and heat source temperature. Second, the condenser outlet state is determined by the heat sink temperature and a vapour quality of 0. Therefore, the condenser pressure is now known. This is also the pressure at the turbine outlet. This pressure combined with the isentropic efficiency of the turbine defines the turbine outlet state. Then, the condenser inlet state is defined by the condensing pressure and a vapour quality of 1. Last, the pump outlet state is found by combining pressure (the same pressure as the turbine inlet) and an increase in enthalpy. This increase in enthalpy is calculated using the pressure head the pump makes and its volumetric flow rate.

3.3.2. Model with recuperator

The recuperator is modelled using the enthalpy difference in the de-superheating process. This is combined with the effectivity of the recuperator heat exchanger and the fact that the mass flow is the same for both sides of the recuperator (as it is a cycle). The recuperated heat is then added between the pump and the evaporator.

3.3.3. Pinch point and heat exchanger sizing

Pinch point is modelled using water as the heat fluid. The water cools linearly as it heats the working fluid. The mass flow rate and the specific heat capacity of water determine the slope of the heat source temperature line. The entropy of the fluid at the evaporator inlet is determined by its thermodynamic state. From there the pinch point is evaluated. It must be positive to ensure no negative heat flow.

Heat exchanger sizing is calculated using its UA-value as a proxy for size. The evaporator is split up in three parts for subcritical cycles (preheater, evaporator and superheater), and two parts for supercritical cycles (preheater and superheater). The separate UA-value of all these parts is calculated using the LMTD method and the correction method of Fakheri (see paragraphs 2.5.2.1. – 2.5.2.2.). They are then added together to form the final UA-value of the evaporator. The sizing of the condenser is also done with the LMTD-method. In the LMTD-method, heat source temperature and working fluid temperature at specific points are needed. Heat source temperatures are calculated using the slope of the heat source temperature line. The working fluid temperatures are derived from the state of the fluid at specific points. These points are the in- and outlets of the different heat exchangers.

3.3.4. Heat exchanger losses and piping losses

Heat exchanger shell side pressure drops are calculated using the Kern method (see paragraph 2.5.2.5.). This is only done for the single phase pressure drops. Two phase pressure drops are not calculated. Piping pressure losses are calculated using the Darcy-Weisbach equations and the Moody diagram (see table 3).

3.3.5. Assesment criteria

To assess the model, the cycle efficiency is used. Cycle efficiency is defined as the ratio of net power output to heat power input. Net power output is defined as the turbine power minus pump power. Heat power is the amount of heat, the heat source provides to the cycle. The metric of cycle efficiency is used to compare working fluids as well as ideal pressure ratios.

Another tool to assess the model are the UA-values of the heat exchangers. Larger UA values indicate a greater size heat exchanger and thus a larger installation cost. The UA value is plotted against cycle efficiency to find the optimal techno-economic working conditions of the cycle.

4. Results

4.1. Initial selection of working fluids

In the baseline model, different working fluids are initially selected (isobutane, isobutene, butene and R236ea), modelled separately and then compared with each other. This initial selection of working fluids is made according to the operating temperature of the system, and the working fluids suggested by Wang et al (Wang, Ling, & Peng, 2012). Table 4 presents the main considerations of each working fluid, namely: ODP, GDP, flammability and toxicity. The table shows that GWP and ODP levels of Isobutane are acceptable according to modern refrigerant standards (GWP below 150 and ODP of 0). The GWP and ODP of Isobutene and Butene are characterised as n.a. because there is currently no information available on it in the ASHRAE Handbook. R236ea is the only refrigerant that is known to exceed the max GWP of 150 by a substantial amount. Still, R236ea is the only working fluid that scores low on the ASHRAE flammability index, categorised to have no flame propagation and therefore considered to be quite safe in terms of flammability. The toxicity of all four initially selected working fluids are also within acceptable levels, with the ASHRAE standard categorising them as low in toxicity. The characteristics of these fluids are shown in table 2.

Table 2: Comparison of working fluid characteristics (ASHRAE, 2021)

Working fluid	GWP	ODP	AHRAE toxicity	ASHRAE flammability
Isobutane	20	0	Low	High
R236ea	1370	0	Low	No flame propagation
Isobutene	n.a.	n.a.	Low	High
Butene	n.a.	n.a.	Low	High

4.2. Baseline model

The following step is to build a baseline of the organic Rankine cycle in Python. This model is based on a set of equations derived from the literature and describes the basic relationships present in an ORC. These equations are shown in table 3.

Using this set-up, a first model is constructed. The model is plotted in a Ts and a logPh diagram for the different initially selected working fluids. These are shown in figures 12a-d and 13a-d. The figures show the characteristic shape of an ORC. From these figures it is clear that all workings fluids operate sub-critically at 30 bar and turbine inlet temperature of 145°C. In addition, these figures also show that all workings fluids are super-heated in this cycle before they are expanded.

Figure 14 shows the relationship between cycle efficiency and temperature for the different working fluids. It is clear that without the recuperator, the butene cycle is the most performant. A possible explanation is that the butene and isobutene cycles need less de-superheating (see figures 12 a-d), so more power is extracted through the expander. This is also shown on the LogPh-diagrams, where the difference in enthalpy

of the de-superheating is greater in the isobutane and R236ea cycles. Furthermore, the efficiencies of the R236ea, butene and isobutene cycles drop to zero for temperature below a certain threshold, as the temperature is not high enough to evaporate these fluids at the given pressure – 30 bar.

Figure 15 shows the ideal pressure for the given turbine inlet temperature. It shows that for isobutane the highest cycle efficiency is reached for a turbine inlet pressure of 39 bar. For R236ea, the optimal cycle efficiency is reached at 35 bar. And butene and isobutene reach there optimal cycle efficiency at 36 bar and 37 bar respectively.

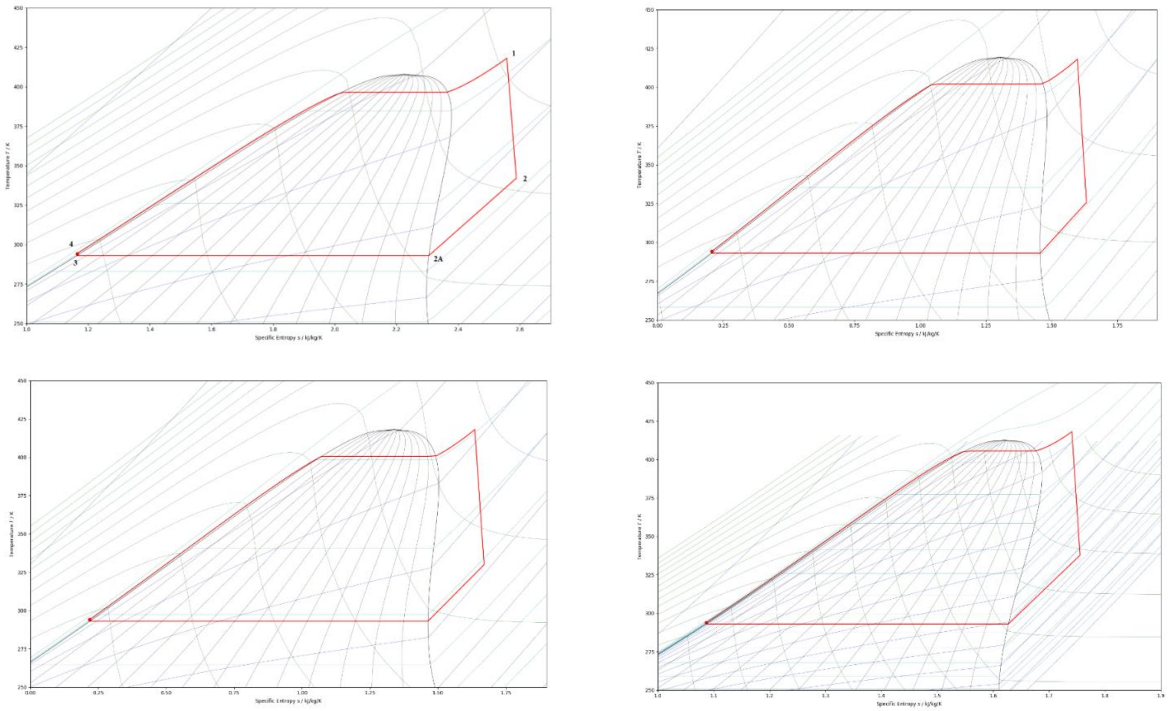

Figure 12a-d: baseline model without recuperator at 30 bar (Ts diagram: Isobutane – Butene – Isobutene – R236ea)

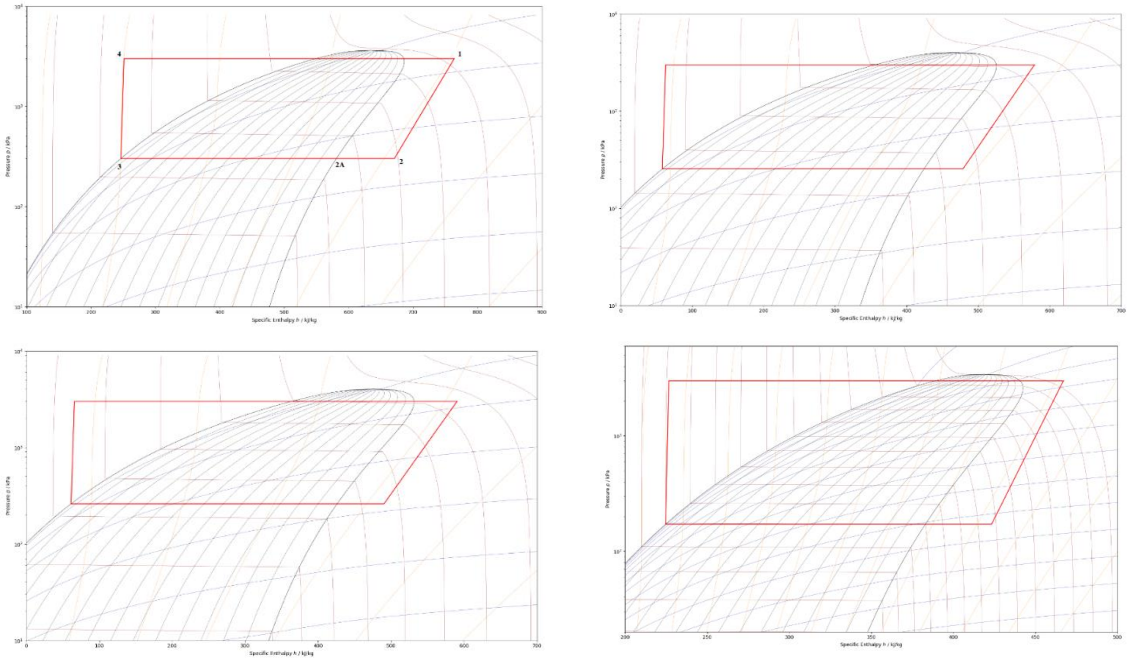

Figure 13a-d: baseline model without recuperator at 30 bar (logPh diagram: Isobutane – Butene – Isobutene – R236ea)

Table 3: list of fundamental equations of the model

	Equations
Pump Power	$P_{pump} = \frac{\dot{m} * (h_4 - h_3)}{\eta_{pump}}$
Turbine Power	$P_{turbine} = \dot{m} * (h_1 - h_2) \quad with \quad h_2 = h_1 - \eta_{isen} * (h_1 - h_{2\_ideal})$
Net Power	$P_{net} = P_{turbine} - P_{pump}$
Heat Input	$\dot{Q}_{in} = \dot{m} * (h_1 - h_4)$
BWR	$BWR\ (\%) = 100\% * \frac{P_{pump}}{P_{turbine}}$
Carnot Efficiency	$\eta_{carnot} = 1 - \frac{T_3}{T_1}$
Cycle Efficiency	$\eta_{cycle} = \frac{P_{net}}{\dot{Q}_{in}}$
Recuperator Heat	$\Delta h_{recup} = (h_2 - h_{2a}) * \eta_{recup}$
Single-Phase Pressure Drop of Heat Exchanger	$\Delta p_{shell-single-phase} = \frac{\rho_s v_s^2}{2} * \frac{L}{B} * \frac{D_s}{D_e} * f_s$
Single-Phase Pressure Drop of piping	$\Delta P = \rho g h_f \quad with \quad h_f = \sum_i K_i \cdot \frac{u_i^2}{2g}$
Heat Loss Piping	$\dot{Q} = L \cdot \frac{(T_1 - T_2)}{R_{per\ meter}}$; $R_{per\ meter} = \frac{1}{2\pi r_1 h_1} + \frac{\ln \frac{r_2}{r_1}}{2\pi \lambda_{12}} + \frac{\ln \frac{r_3}{r_2}}{2\pi \lambda_{23}} + \frac{1}{2\pi r_3 h_3}$

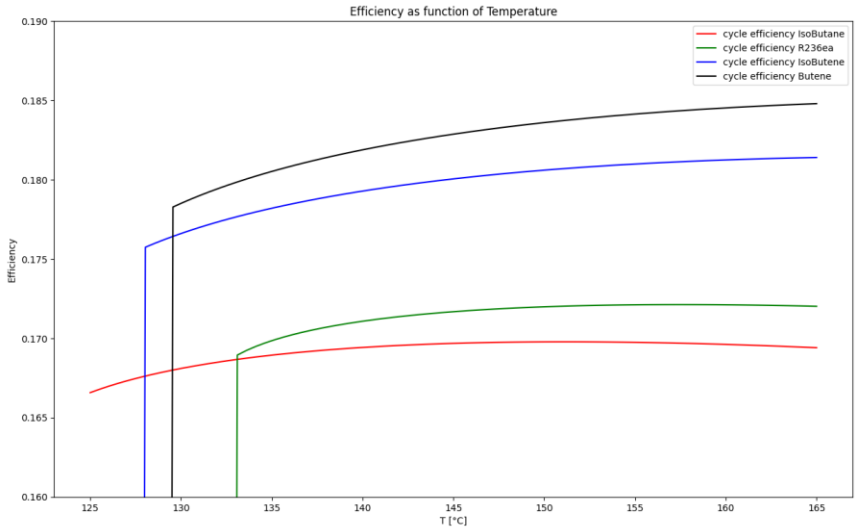

Figure 14: Comparison of working fluids across a temperature range without recuperator (with P = 30bar)

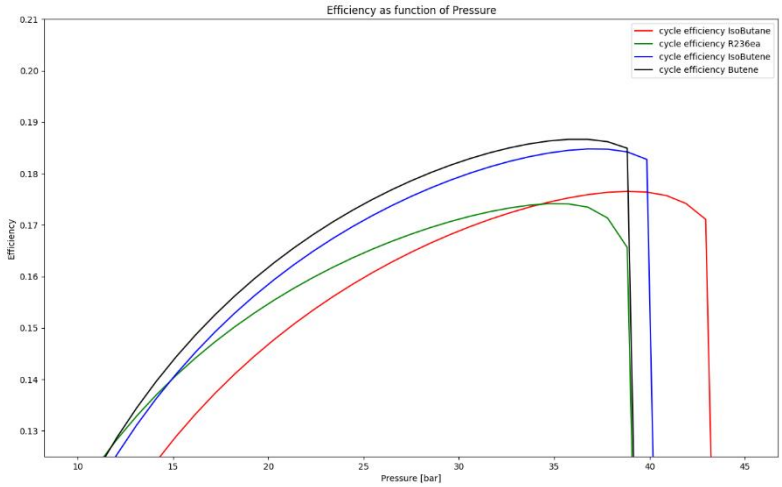

Figure 15: Comparison of working fluids across turbine inlet pressure without recuperator

4.3. Model with recuperator and working fluid selection

The next step in building the ORC model is to add the recuperator to the cycle. The recuperator recuperates heat at the exhaust of the expander and transfers it to the fluid just after the pump. The cycle efficiencies with the recuperator are shown in figure 16. It comes as no surprise that the efficiency increases (by about 3 percent in the case of isobutane). Especially the working fluids that require more de-superheating will benefit from the recuperator. This can be seen in the T-s diagrams of said fluids (figures 12 a-d). The de-superheating happens between points 2 and 2a in the T-s diagrams (see figure 12a).

For example, in the case of isobutane, the recuperator heats the working fluid back up from 21.3°C to 52.2°C. This is energy the heat source no longer needs to supply, hence a more efficient cycle. The cycle efficiencies of the different working fluids with the recuperator yield very similar results, in comparison with each other.

Figure 16 shows the ideal pressure for the given turbine inlet temperature. Relative to the ideal pressures of the cycle without a recuperator, the ideal pressures are now slightly lower. This may be because, as the pressure rises, less de-superheating is necessary, so less energy is recuperated.

From figures 16 and 17, the optimal working fluid is derived. The figures show that the different working fluids are highly similar in terms of cycle efficiency. Therefore, the other main characteristics of the working fluid are important to compare as well. From this comparison, isobutane is selected as the final ORC working fluid. Isobutane has a low GWP of 20, an ODP of 0 and is low in toxicity. These benefits outweigh the downside of having a high flammability (see table 4). Furthermore, isobutane is also a very cheap working fluid, making it the ideal techno-economical choice for this ORC.

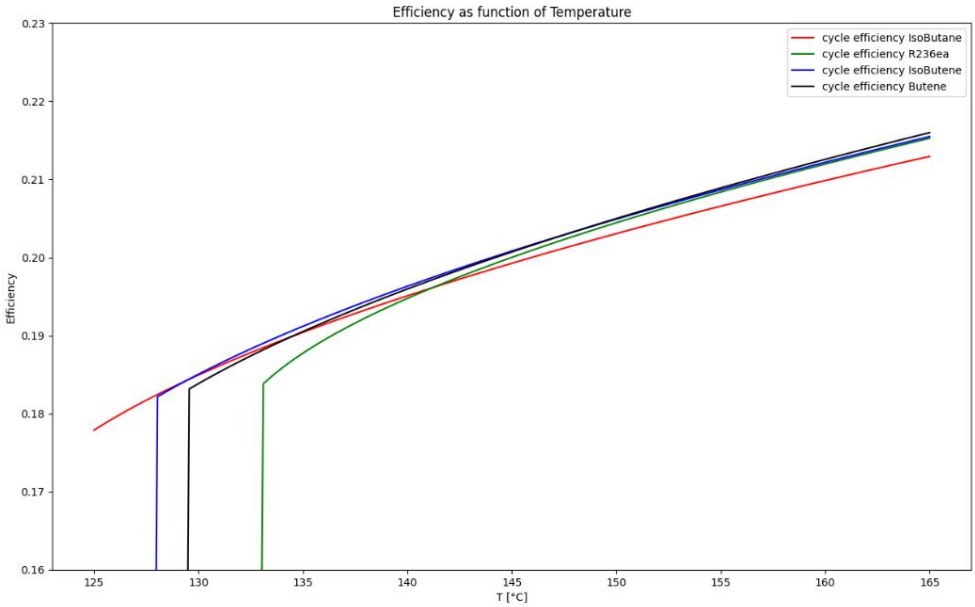

Figure 16: Comparison of working fluids across a temperature range with recuperator (with P = 30 bar)

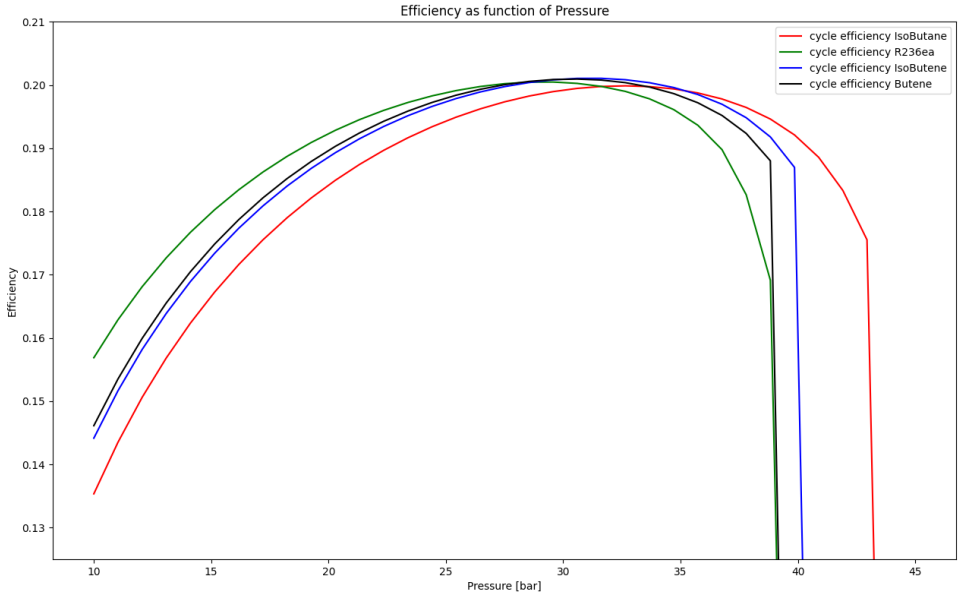

Figure 17: Comparison of working fluids across pressure ratios with recuperator (With $T_{turbine}$ = 145°C)

4.4. Effect of heat exchanger losses, piping losses and pinch point

Next, the associated shell side single-phase pressure drops are derived using the Kern method for shell and tube heat exchangers (see table 4). The piping pressure losses are also calculated. The cycle efficiency without pressure losses is 0.1995. With said pressure losses, the cycle efficiency is 0.1993. The pressure losses are therefore found to be negligible.

Then, the pinch point of the cycle at the hot source side is evaluated. For this, the cycle is presented in a T-s diagram (see figure 18). The final pinch point temperature difference amounts to 3K, ensuring no negative heat flow. Furthermore, as the temperature differences between both fluids in the heat exchanger remain relatively low, there is no concern for departure from nucleate boiling in the heat exchanger.

Table 4: Heat exchanger characteristics and shell side pressure drops

Component	UA-value $[\frac{kW}{K}]$	$\dot{Q}_{trans}$ $[kW]$	ΔP [Pa]
(1) Preheater	60.76	1038	4,412
(2) Evaporator	73.60	672	/
(3) Superheater	37.39	387	25418
(4) Recuperator	27.21	441	1153
(5) Condenser	157.86	1,625	/
Total of (1), (2) & (3)	171.74	2,098	29830
Piping	/	0.176	235

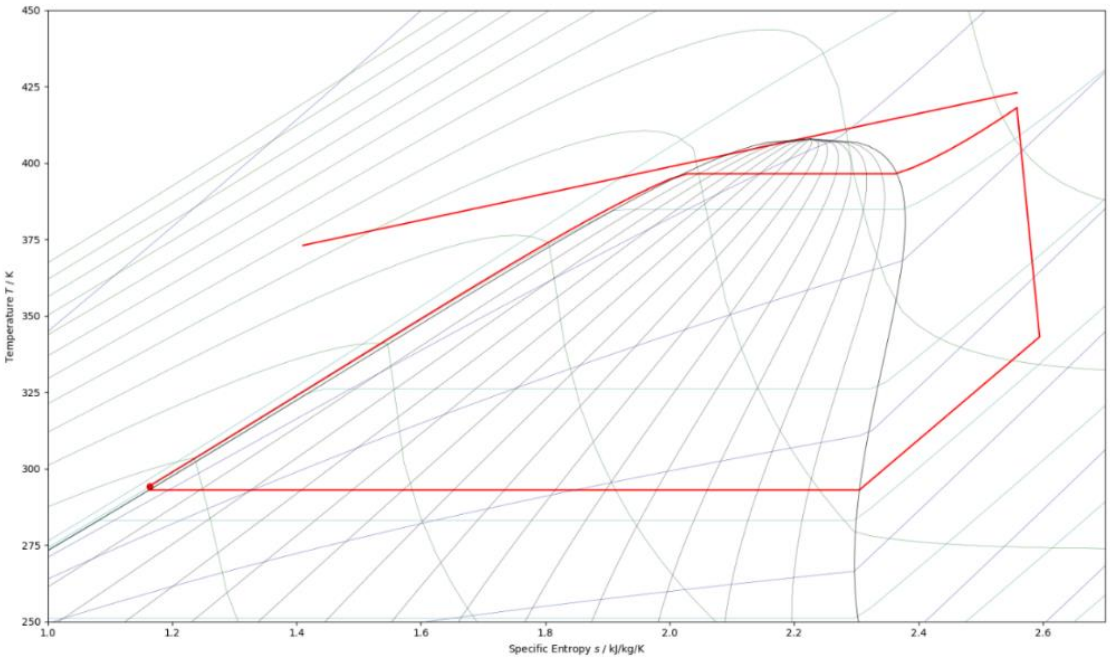

Figure 18: T-s diagram of isobutane and its pinch point at 30 bar

4.5. Heat exchanger size & cycle efficiency

In previous model iterations, cycle efficiency is used to compare different results. Although cycle efficiency is an important parameter in any power cycle, other aspects of the cycle such as installation cost are often at least as important. In this section of the model, the trade-off between both is discussed by looking at the heat exchanger size and the associated cycle efficiency. The UA value of the heat exchanger is used as a proxy for its size, giving an indication of its potential cost. This relationship of installation cost and cycle efficiency is examined for a changing pressure ratio and for a changing turbine inlet temperature (with the heat source temperature remaining constant).

The adjusted total UA values and the heat power Q-values are calculated for the different heat exchangers (see table 6). Furthermore, figure 19 shows a 4D-plot of cycle efficiencies as functions of turbine inlet temperature and pressure, with the UA-values shown as the colour of the surface. There is a small discontinuity, as at 36.47 bar the critical pressure of isobutane is reached. There, the model transitions from a three part heat exchanger (preheater, evaporator, superheater) to a two part heat exchanger (preheater, superheater), as the cycle goes supercritical. At the highest turbine inlet temperature (145 °C), the cycle efficiency rises marginally after 30 bar, and eventually even declines. The UA-value, however, still increases rapidly after 30 bar . Therefore, from a techno-economic standpoint, a turbine inlet temperature and pressure of 145 °C and 30 bar respectively are considered to be the optimal parameters. The UA-value at this point amounts to 172 kW/K. Figures 20 (a) and (b) show cycle efficiency and UA values of the evaporator at 135°C and 145°C as a function of pressure. These figures show that initially the cycle's efficiency tends to increase more rapidly than the UA-values of the heat exchanger when temperature or pressure increases towards its optimal state. However, after some increase in temperature or pressure, the UA values increase more rapidly than the cycle efficiency (especially in the case of temperature). This indicates that there is in fact a trade-off present between installation cost and cycle efficiency and that this trade-off becomes less beneficial as the optimal cycle efficiency is approached.

This analysis is repeated for the condenser. Originally, a UA value of around 302 kW/K was found. If one were to increase the condensation temperature of the fluid by 5K (to 25 °C), the cycle efficiency declines from 0.1995 to 0.1906. The UA-value of the condenser however, almost halves(!) to 158 kW/K. This again indicates that potentially large installation cost savings can be made by diverting slightly from the optimal cycle efficiency conditions. The efficiency of the final cycle is 19%, and this amounts to a second law efficiency of 58%. Additionally, to achieve the required 400kW of mechanical power, a mass flow of hot geothermal water of 9.85 kg/s is used, which falls within the limit of the case study of 10 kg/s.

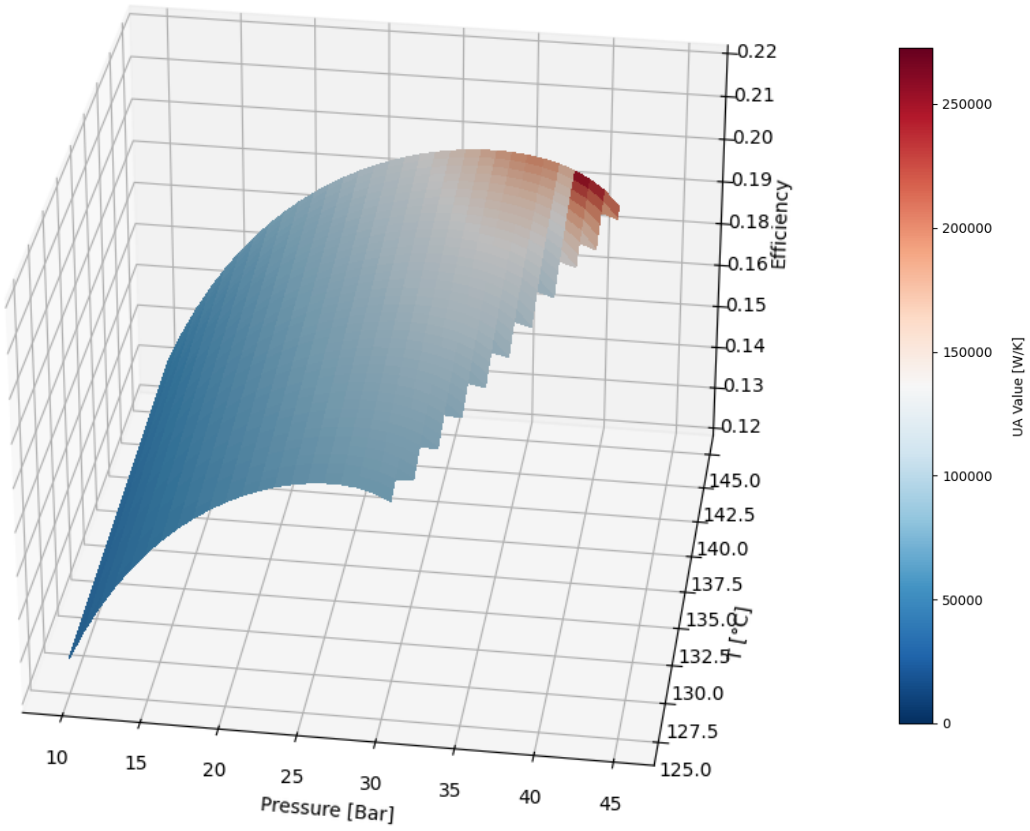

Figure 19 : 4D-plot of cycle efficiency using isobutane and UA-values as face colour

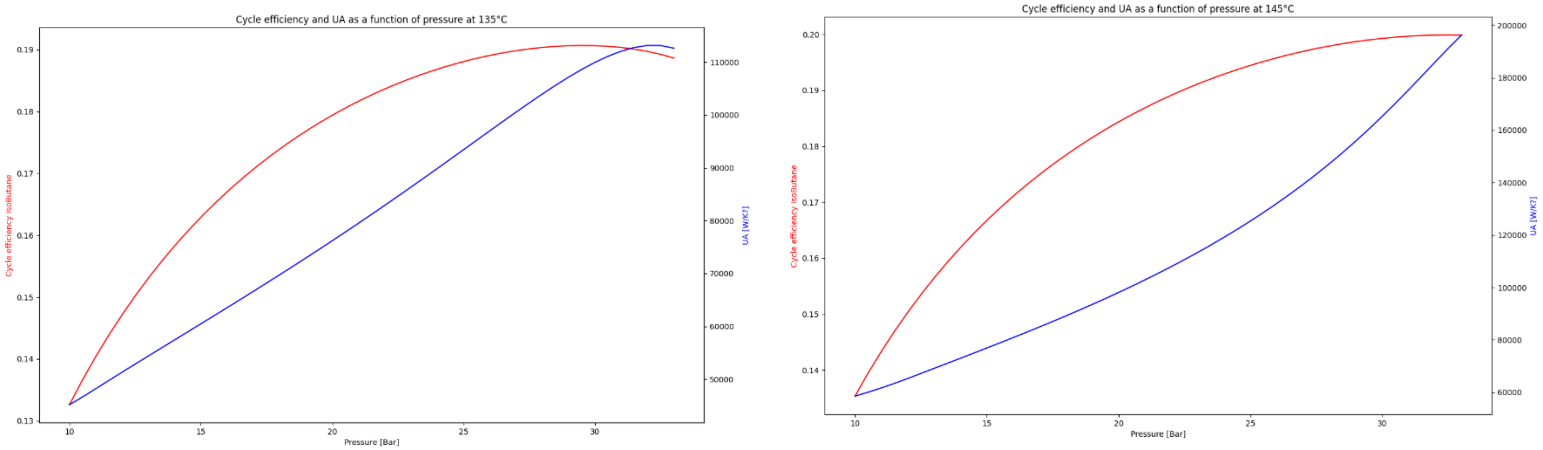

Figures 20 (a,b): cycle efficiency and UA values of the evaporator at 135°C and 145°C

4.6. Sensitivity analysis

Small pressure fluctuations do not have a big impact on cycle efficiency. Only when the pressure drops below about 25 bar, does the cycle efficiency significantly decline. Small temperature fluctuations do not have a big impact on cycle efficiency either. This can be seen in figure 21. What does have a major impact though, is the turbine isentropic efficiency. This can be seen in figure 22. This figure shows an almost linear correlation between cycle- and turbine efficiency. Variations on isentropic efficiency thus have a significant impact on cycle efficiency. It is imperative then to have a turbine with the highest possible efficiency.

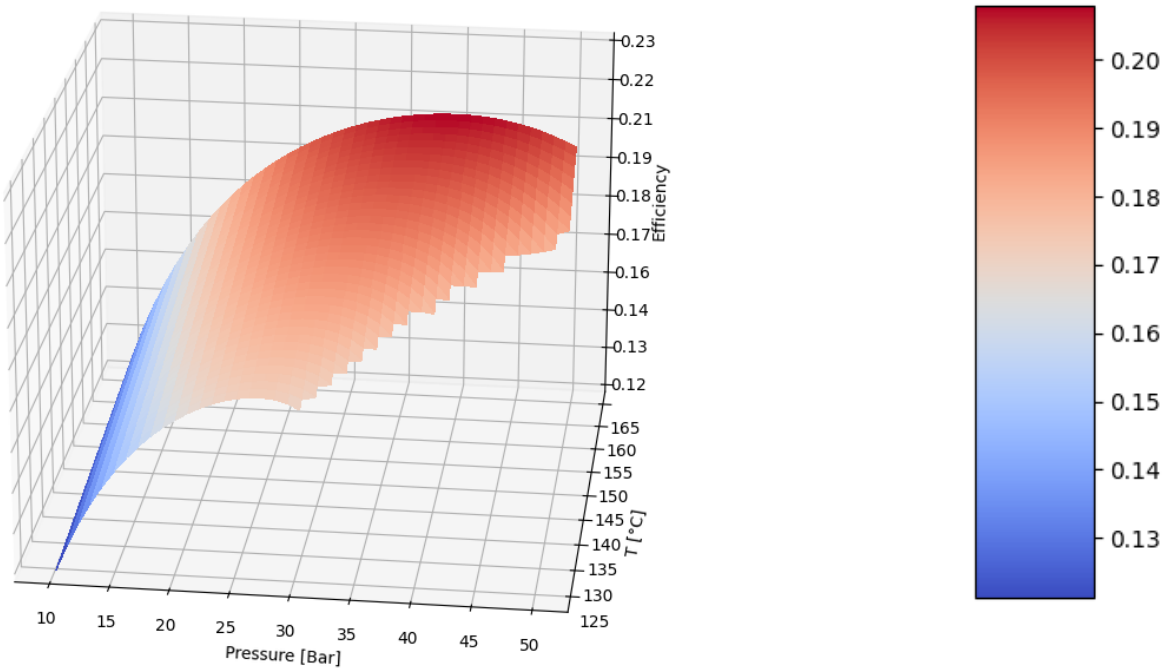

Figure 21: Heat source temperature variation and corresponding ideal pressure ratio

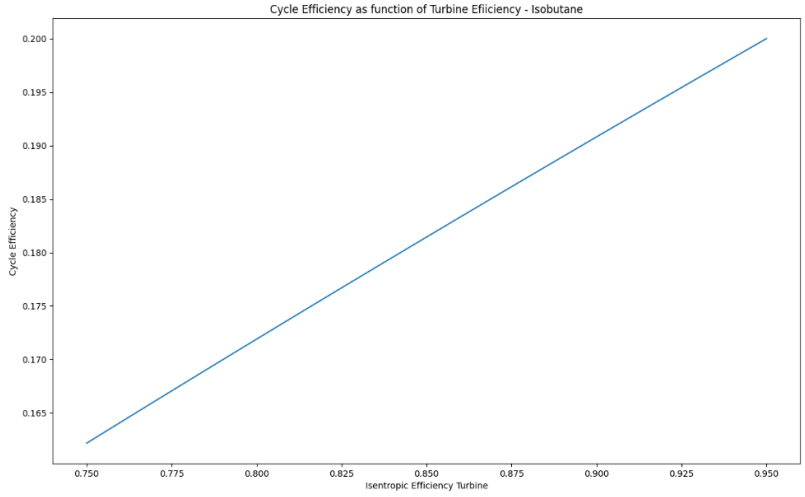

Figure 22: Effect of turbine isentropic efficiency on cycle efficiency

4.7. Validation and limitations

Wang et al. looked at cycle efficiencies for a selection of working fluids and found thermal efficiencies in the range of 18-23% and an exergy efficiency in the range of 60-75% (Wang D. , Ling, Peng, Liu, & Tao, 2013). Equivalent results were found by Lai et al., pinning exergy efficiency at 70% (Lai, Wendland, & Fischer, 2011). Liu et al. also came to similar results, concluding that thermal efficiency for the given expander inlet temperature of 145°C falls within the range of 15-20% (Liu, Chien, & Wang, 2004). These results are in line with what this paper found, i.e. a thermal efficiency of 19% and an exergy efficiency of 58%.

However, some clear limitations are still present within the analysis of the paper. A first way the analysis can be expanded is by considering the total efficiency of the power plant, i.e. the power losses on the heat source and heat sink side of the cycle. For example by considering the pump power consumption of both sides. A second way to further improve the analysis is by expanding the pressure drop examination of the heat exchangers. In the current model, only single-phase shell side pressure drops are considered. However, two-phase pressure drops on the shell side and single-and two-phase pressure drops on the tube side of the heat exchanger could also be considered. Another limitation is the absence of subcooling. When the fluid reaches a vapour quality of 0, it is pumped up. In reality however, the fluid would be subcooled, to ensure that the fluid goes through the pump completely as a liquid. A fourth limitation is the lack of empirical results on the cycle. All results presented in the paper are derived from theoretical models without the addition of self-collected data or industry data. Contact had been made with someone at the geothermal energy plant of Balmatt in Mol for the collection of data. However, it was impossible to schedule a date in time. Nonetheless, we will still visit Balmatt even though this paper will have been submitted by then.

Other ways to expand the analysis without changing the current model are for example to look at the effect of superheating on the turbine power and size. Or, for example to consider the effect of the pinch point of the condenser at the heat sink side instead of focussing only on the pinch point in the evaporator at the heat source.

5. Conclusions

Four working fluids were selected for the optimisation of a geothermal (150°C) ORC cycle of 400 kW. Analysis were carried out on ideal temperature, pressure ratios and the presence of a recuperator. The recuperator showed to be highly effective in increasing the cycle efficiency. Pressure losses in piping and heat exchangers were found to be negligible. Isobutane was selected as the working fluid due its low GWP, zero ODP, low cost and its properties in the given temperature range. Cycle efficiency and installation costs were shown to have an inverse relationship, influenced by the size of the heat exchangers. The sensitivity analysis showed that results were robust for small changes in temperature and pressure. However, the results were influenced substantially by changes in the isentropic efficiency of the turbine.

From a techno-economic standpoint, the most optimal cycle had a cycle efficiency of 19%, which amounts to a second law efficiency of 58%. This was achieved by using isobutane (R600a) as a working fluid, with turbine inlet and outlet temperature and pressure of 145 °C and 30 bar, and 73 °C and 3.5 bar, respectively.

6. References

Abboud, H., & Khoury, P. (2015). *Conception and design of a solar driven Stirling engine for electrical generation*. Beirut.

Agemar, T., Weber, J., & Schulz, R. (2014). Deep Geothermal Energy Production in Germany. *Energies*, 4397-4416.

Ahmadi, M. H., Ghazvini, M., Sadeghzadeh, M., Alhuyi Nazari, M., Kumar, R., Naeimi, A., & Ming, T. (2018). Solar power technology for electricity generation: A critical review. *Energy Science & Engineering, 6*, 340-361.

Allessandra, R. (2023, July 21). *Concentrated Solar Power (CSP) versus Photovoltaic (PV): an in-depth comparison*. Retrieved from solarfeeds: https://www.solarfeeds.com/mag/csp-and-pv-differences-comparison/

Ármannsson, H. (2003). CO2 emission from Geothermal Plants. *International Geothermal Conference.* Reykjavík.

ASHRAE. (2021). *ASHRAE Handbook.* Peachtree corners, Georgia, US.

Badr, O., S., D. P., & P., W. O. (1985). Selecting a working fluid for a Rankine-cycle engine. *Applied Energy*, 1-42.

Bahrami, M. (2020). *Vapor Power Cycles.* Retrieved 12 13, 2023, from https://www.sfu.ca/~mbahrami/ENSC%20461/Notes/Vapor%20Power%20Cycles.pdf

Bahrami, M., Pourfayaz, F., & Kasaeian, A. (2022). Low global warming potential (GWP) working fluids (WFs) for Organic Rankine Cycle (ORC) applications. *Energy Reports, 8*, 2976-2988.

Brazetek. (2012). *Parallel Flow Heat Exchangers*. Retrieved from brazetek.com: https://www.brazetek.com/articles/112-parallel-flow-heat-exchangers#:~:text=Thus%2C%20parallel%20flow%20in%20heat,recommended%20to%20solve%20these%20problems.

Brennen, C. E. (2005). *Fundamentals of Multiphase Flow.* Pasadena: Cambridge University Press.

Butterfield, J. L., Gillette, A. B., & Shin, R. (2014). *Goethermal Energy (Five Activities).* US Department of Energy: Energy Efficiency & Renewable Energy.

Campana, F., Bianchi, M., Branchini, L., De Pascale, A., Peretto, A., Baresi, M., . . . Vescovo, R. (2013). ORC waste heat recovery in European energy intensive industries: Energy and GHG savings. *Energy Conversion and Mangement, 76*, 244-252.

Chen, Y., Liu, Y., & Liu, W. (2021). Optimal design of radial inflow turbine for ocean thermal energy conversion based on the installation angle of nozzle blade. *Renewable Energy*, 857-870.

CoolProp. (2023). *Fluid Properties*. Retrieved from CoolProp.org: http://www.coolprop.org/fluid_properties/index.html

Dambly, B. W., & Lyman, S. R. (1982). The organic rankine cycle for geothermal power generation. *Energy, Resources and Environment*, 322-329.

Dass, N. H. (2021). *Essentials of Thermodynamics.* SRI Books: the Simplicity Research Institute.

Delgado-Torres, A. M. (2018). Effect of ideal gas model with temperature-independent heat capacities on thermodynamic and performance analysis of open-cycle gas turbines. *Energy conversion and management, 176*, 256-273.

Demirel, Y., & Gerbaud, V. (2019). *Nonequilibrium Thermodynamics.* Elsevier.

Desai, N. B., & Bandyopadhyay, S. (2016). Thermo-economic analysis and selection of working fluid for solar organic Rankine cycle. *Applied Thermal Engineering, 95*, 471-481.

Dick, E. (2015). *Fundamentals of Turbomachines.* Dordrecht, The Netherlands: Springer.

Dimain, A. C., Bildea, C. S., & Kiss, A. A. (2014). *Computer Aided Chemical Engineering: Integrated Design and Simulation of Chemical Processes* (Vol. 13). Elsevier Science.

Dincer, I. (2018). *Comprehensive Energy Systems.* Elsevier.

Enerquip. (2018, March 12). *What's the difference between parallel flow, counter flow and crossflow heat exchangers?* Retrieved from Enerquip.com: https://www.enerquip.com/whats-the-difference-between-parallel-flow-counter-flow-and-crossflow-heat-exchangers/#:~:text=The%20inlet%20temperatures%20of%20the,other%20flow%20patterns%2C%20Thermopedia%20noted.

Ennio, M., & Astolfi, M. (2016). *Organic rankine cycle (ORC) power systems: technologies and applications.* Woodhead Publishing.

European Comission. (2023, February). *Climate Action*. Retrieved from Europa.eu: https://climate.ec.europa.eu/eu-action/ozone-layer/overview_en#:~:text=Ozone%20layer%20depletion%20causes%20increased,cataracts%20and%20immune%20deficiency%20disorders.

European Environment Agency. (2023, august 10). *Glossary: Global-warming potential (GWP)*. Retrieved from Eurostat: https://ec.europa.eu/eurostat/statistics-explained/index.php?title=Glossary:Global-warming_potential_(GWP)#:~:text=Global%2Dwarming%20potential%2C%20abbreviated%20as,remains%20active%20in%20the%20atmosphere.

Exergy-ORC. (2022). *Waste heat recovery systems from industrial process*. Retrieved from Exergy-orc.com: https://www.exergy-orc.com/

Feng, X., Li, H., & Huang, J. (2023). Structural Design and Analysis of a 100 kW Radial Turbine for an Ocean Thermal Energy Conversion–Organic Rankine Cycle Power Plant. *Processes*.

Ferrara, F., Gimelli, A., & Lunogo, A. (2014). Small-scale concentrated solar power (CSP) plant: ORCs comparison for different organic fluids. *Energy Procedia, 45*, 217-226.

Forman, C., Muritala, I., Pardemann, R., & Meyer, B. (2016). Estimating the global waste heat potential. *Renewable and Sustainable Energy Reviews*, 57.

Fridleifsson, I. R. (2008). The possible role and contribution of geothermal energy to the mitigation of climate change. *IPCC Scoping Meeting on Renewable Energy Sources*.

Garg, P., Orosz, M. S., & Kumar, P. (2016). Thermo-economic evaluation of ORCs for various working fluids. *Applied Thermal Engineering, 109*, 841-853.

Gronnerud, R. (1974). *Two-phase flow resistance in boiling refrigerants.* Kjoleteknik: Norges tekn Hogskole Inst.

Hall, C., & Dixon, L. S. (2013). *Fluid mechanics and thermodynamics of turbomachinery*. Butterworth-Heinemann.

Hereijgers, J. (2021). *Fluïdummechanica.* Antwerpen: Universiteit Antwerpen.

Hertwich, E. G., Mateles, S. F., Pease, W. S., & McKone, T. E. (2001). Human toxicity potentials for life-cycle assessment and toxics release inventory risk screening. *Environmental Toxicology and Chemistry, 20*, 928-939.

HRS. (2024). *Fouling Factors in Heat Exchangers*. Retrieved from hrs-heatexchangers.com: https://www.hrs-heatexchangers.com/resource/fouling-factors-in-heat-exchangers/#:~:text=When%20this%20type%20of%20fouling,high%2Dpressure%20water%20jets).

Hung, T. C., Shai, T. Y., & Wang, S. K. (1997). A review of organic Rankine cycles (ORCs) for the recovery of low-grade waste hea. *Energy*(7), 661-667.

Ibrahim, D. (2018). *Comprehensive energy systems.* Elsevier.

ICGC. (2011). *The origin of the Earth's heat*. Retrieved from Institut Cartogràfic i Geològic de Catalunya: https://www.icgc.cat/en/Public-Administration-and-Enterprises/Services/Geothermics/The-origin-of-the-Earth-s-heat#:~:text=%2D%20Kinetic%20or%20friction%20heat%3A%20It,the%20Sun%20(tidal%20forces).

Imran, M. U. (2016). Volumetric expanders for low grade heat and waste heat recovery applications. *Renewable and Sustainable Energy Reviews*, 1090-1109.

International Energy Agency. (2024). *Solar PV*. Retrieved from IEA: https://www.iea.org/energy-system/renewables/solar-pv

IRENA: International Renewable Energy Agency. (2012). *RENEWABLE ENERGY TECHNOLOGIES: COST ANALYSIS SERIES.* IRENA.

Jaffe, R. L., & Taylor, W. (2018). *The physics of energy.* Cambridge University Press.

Janssen, E. (2022). *Pompen en compressoren.* Antwerpen: Universiteit Antwerpen.

Jiménez-García, J., Ruiz, A., Pacheco-Reyes, A., & Rivera, W. (2023). *A Comprehensive Review of Organic Rankine Cycles.* Retrieved from https://www.mdpi.com/2227-9717/11/7/1982

Junjiang, B., & Zhao, L. (2013). A review of working fluid and expander selections for organic Rankine cycle. *Renewable and sustainable energy reviews, 24*, 325-342.

Kagel, A., Bates, D., & Gawell, K. (2005). *A guide to geothermal energy and the environment.* Washington: Geothermal Energy Association.

Khansefid, A., Yadollahi, S. M., Müller, G., & Taddei, F. (2022). Induced Earthquake Hazard by Geothermal Power Plants: Statistical Evaluation and Probabilistic Modeling. *International Journal of Disaster Risk Science*, 758-777.

Klimaszewski, P., & Klonowicz, P. (2020). Design and performance analysis of ORC centrifugal pumps. *Archives of Thermodynamics*, 203-222.

Kosmadakis, G. (2024). Industrial waste heat potential and heat exploitation solutions. *Applied Thermal Engineering, 246.*

Kumar, I. N., Bhatti, S. K., Krishna, C. M., Vundru, C., & Neelapu, M. L. (2006). *Avanced Computational Methods in Heat Transfer IX.* WitPress.

Lai, N., Wendland, M., & Fischer, J. (2011). Working fluids for high-temperature organic Rankine cycles. *Energy*, 1999-211.

Lara-Montaño, O. D., Gómez-Castro, F. I., & Gutiérrez-Antonio, C. (2020). Development of a virtual environment for the rigorous design and optimization of shell-and-tube heat exchangers. *Computer Aided Chemical Engineering*, 19-24.

Larjola, J. (1995). Electricity from industrial waste heat using high-speed organic Rankine cycle (ORC). *International Journal of Production Economics*, 227-235.

Linquip Team. (2023, June 18). *Linquip Technews*. Retrieved from What is Cross Flow Heat Exchangers and its Working Principles: https://www.linquip.com/blog/cross-flow-heat-exchangers/

Linteris, G. T., Bell, I. T., & Mclinden, M. O. (2019). An empirical model for refrigerant flammability based on molecular structure and thermodynamics. *International Journal of Refrigeration, 104*, 144-150.

Liu, B.-T., Chien, K.-H., & Wang, C.-C. (2004). Effect of working fluids on organic Rankine cycle for waste heat recovery. *Energy*, 1207-1217.

Loewer, M., & Keim, M. (2022). *Renewable Energy Production and Distribution* (Vol. 1). Academic press.

Manente, G., Lazzaretto, A., & Bonamico, E. (2017). Design guidelines for the choice between single and dual pressure layouts in organic Rankine cycle (ORC) system. *Energy, 123*, 413-431.

Marcuccilli, F., & Mathiasin, H. (2006). Kalina & Organic Rankine Cycles: How to Choose the Best Expansion Turbine? *Electricity Generation from Enhanced Geothermal Systems*.

Matuszewska, D. (2020). Molecular Complexity of Working Fluids Dedicated to Organic Rankine Cycle (ORC. *IOP Conference Series: Materials Science and Engineering, 946*.

Mehdizadeh-Fard, M., Pourfayaz, F., & Maleki, A. (2021). Exergy analysis of multiple heat exchanger networks: An approach based on the irreversibility distribution ratio. *Energy Reports*, 174-193.

Moran, M. J., Shapiro, H. N., Boettner, D. D., & Bailey, M. B. (2010). *Fundamentals of engineering thermodynamics.* John Wiley & Sons.

Nimish Shah. (2014, 04 16). *LMTD Correction Factor*. Retrieved from Sistemas.eel.usp.br: https://sistemas.eel.usp.br/docentes/arquivos/5817712/LOQ4086/lmtd.correction.factor.pdf

Norton, D. J. (2016). The impossible process: Thermodynamic reversibility. *Studies in History and Philosophy of Science Part B: Studies in History and Philosophy of Modern Physics*, 43-61.

Noughabi, A. K., & Sammak, S. (2018). Detailed Design and Aerodynamic Performance Analysis of a Radial-Inflow Turbine. *Applied Sciences*.

Nuclear Power. (2024, March 29). *DNB – Departure from Nucleate Boiling*. Retrieved from nuclear-power.com: https://www.nuclear-power.com/nuclear-engineering/heat-transfer/boiling-and-condensation/dnb-departure-from-nucleate-boiling/

Nuclear Power. (2024, March 25). *Flow Boiling – Forced Convection Boiling*. Retrieved from nuclear-power.com: https://www.nuclear-power.com/nuclear-engineering/heat-transfer/boiling-and-condensation/flow-boiling-forced-convection-boiling/

Ohji, A., & Haraguchi, M. (2017). Steam turbine cycles and cycle design optimization: the Rankine cycle, thermal power cycles, and IGCC power plants. *Advances in steam turbines for modern power plants*, 11-40.

Pan, L., & Shi, W. (2016). Investigation on the pinch point position in heat exchangers. *Journal of Thermal Science, 25*, 258-265.

Papapetrou, M., Kosmadakis, G., Cipollina, A., La Commare, U., & Micale, G. (2018). Industrial waste heat: Estimation of the technically available resource in the EU per industrial sector, temperature level and country. *Applied Thermal Engineering*, 207-216.

Pedone Bandarra Filho, E., & Heleno Pontes, A. A. (2016). Experimental investigation on the performance and global environmental impact of a refrigeration system retrofitted with alternative refrigerants. *International Journal of refrigeration,, 70*, 119-127.

Pettinato, B., Rainer, K., & Leonid, M. (2022). *Machinery and Energy Systems for the Hydrogen Economy.* Elsevier.

Primo, J. (2020). *Shell and Tube Heat Exchangers - Basic.* Retrieved from PHD Online: https://www.pdhonline.com/courses/m371/m371content.pdf

Quoilin, S. (2007). *Experimental Study and Modeling of a Low Temperature Rankine Cycle for Small Scale Cogeneration.* Liège: Université de Liège.

Quoilin, S. (2008). *An introduction to thermodynamics applied to Organic Rankine Cycles.* Cambridge: Massachussetts Institute of Technology.

Quoilin, S. (2009). *An introduction to thermodynamics applied to organic rankine cycles.* Liège: Université de Liège.

Quoilin, S. (2011). *Sustainable energy conversion through the use of Organic Rankine Cycles for waste heat recovery and solar applications.* Liège: University of Liège.

Roetzel, W., Luo, X., & Chen, D. (2019). *Design and Operation of Heat Exchangers and their Networks.* Elsevier.

Rops, C., Hossain, T., & Boerboom, P. (2021). *ORC System Optimisation: innovative exhaust heat exchanger, in-engine block heat exchanger and zero impact condensor.* Munich: 6th International Seminar on ORC Power Systems.

Roy, J. P., Mishra, M. K., & Misra, A. (2011). Parametric Optimization and Performance Analysis of a Regenerative Organic Rankine Cycle Using Low–Grade Waste Heat for Power Generation. *International Journal of Green Energy*, 173-196.

Saari, J. (2010). *Heat exchanger dimensioning.* University of Lappeenranta.

Sacome. (2019, October 21). *Heat Exchanger | Advantages, uses and applications*. Retrieved from Sacome.com: https://www.sacome.com/en/heat-exchanger-advantages-uses-applications/#:~:text=Advantages%20of%20tubular%20heat%20exchangers&text=Low%20maintenance%20costs.,of%20particulate%20or%20fibre%20products.

Sauret, E., & Gu, Y. (2014). Three-dimensional off-design numerical analysis of an organic Rankine cycle radial-inflow turbine. *Applied Energy*.

Sauret, E., & Petrie-Repar, P. (2012). Preliminary Design and Performance Estimation of Radial Inflow Turbines: An Automated Approach. *Journal of Fluids Engineering*.

Scott, E., & Alderton, D. (2021). *Encyclopedia of geology* (Vol. 2nd). Academic Press.

SolarPACES. (2024). *CSP Projects around the world*. Retrieved from SolarPaces: Solar Power & Chemical Energy Systems: https://www.iea.org/data-and-statistics/charts/renewable-electricity-capacity-additions-by-technology-and-segment-2016-2028

Tomarov, G. V., & Shipkov, A. A. (2017). Modern geothermal power: Binary cycle geothermal power plants. *Thermal Engineering, 64*, 243-250.

Triogen. (2024, March 21). *TRIOGEN HIGH-SPEED TURBO GENERATOR*. Retrieved from triogen.nl: http://www.triogen.nl/technology/triogen-high-speed-turbo-generator

UN Environment Programme. (2023). *The Montreal Protcol*. Retrieved from Ozone.unep.org: https://ozone.unep.org/treaties/montreal-protocol

Van de Paer, J. (2022). *Warmteleer*. Antwerpen: Universiteit Antwerpen.

Walraven, D., Laenen, B., & D'haeseleer, W. (2012). *Comparison of Thermodynamic Cycles for Electricity Production from Low-Temperature Geothermal Heat Sources.* Leuven: KUL Energy and Environment.

Wang, D., Ling, X., & Peng, H. (2012). Efficiency and optimal performance evaluation of organic Rankine cycle for low grade waste heat power generation. *Energy*, 343-352.

Wang, D., Ling, X., Peng, H., Liu, L., & Tao, L. (2013). Efficiency and optimal performance evaluation of organic Rankine cycle for low grade waste heat power generation. *Energy*, 343-352.

Wang, Z. (2023). Entropy production analysis of a radial inflow turbine with variable inlet. *Energy*.

Wang, Z., Zhang, Z., & Xia, X. (2019). Preliminary design and numerical analysis of a radial inflow turbine in organic Rankine cycle using zeotropic mixtures. *Applied Thermal Engineering*.

Wheatley, J. C., Gregory, W. S., & Albert, M. (1986). he natural heat engine. *Los Alamos Science*, 2-33.

Williams, Q. (1997, October 6). *Why is the earth's core so hot? And how do scientists measure its temperature?* Retrieved from Scientific American: https://www.scientificamerican.com/article/why-is-the-earths-core-so/#:~:text=There%20are%20three%20main%20sources,the%20decay%20of%20radioactive%20elements.

Xu, J., & Yu, C. (2014). Critical temperature criterion for selection of working fluids for. *Energy, 74*, 719-733.

Yan, D., Yang, F., Yang, F., Zhang, H., & Guo, Z. (2020). Experimental investigation of the pipeline pressure losses effect on ORC. *International Conference on Applied Energy.* Bangkok.

Ye, S., Xu, Y., Chen, Y., & Wei Guang, H. (2020). Analysis of heat transfer and irreversibility of ORC evaporator for selecting working fluid and operating conditions. *Thermal Science*, 2013-2022.

Zhang, H. L., Baeyens, J., Degrève, J., & Cacères, G. (2013). Concentrated solar power plants: Review and design methodology. *Renewable and sustainable energy reviews, 22*, 466-481.

8. Appendices

A. Key thermodynamic concepts

A.a. Thermodynamic heat engine

A thermodynamic heat engine converts thermal energy into mechanical work and vice-versa. Therefore, an idealized heat engine is considered to be functionally reversible. This means it can operate in two modes. The first mode is as a prime mover, where heat is allowed to flow from a high to a low temperature and a portion of that heat is converted into mechanical work. The second mode is as a heat pump, where mechanical work is added to the engine and heat is pumped from a low to a high temperature (Wheatley, Gregory, & Albert, 1986).

Besides functional reversibility, the thermodynamic reversibility of a heat engine also needs to be considered. A reversible thermodynamic process is a process that can change its direction in incremental steps, each step moving from one equilibrium state to another. This means that when considering a prime mover and heat Q_{in} is inputted by the system and work W_{out} is outputted and then the direction is reversed, that work inputted is equal to $W_{in} = -W_{out}$ and heat outputted is equal to $Q_{out} = -Q_{in}$. Thus, a heat pump is created with identical but reversed results to the prime mover (Norton, 2016). However, to achieve thermodynamic reversibility, the process has to obey some practically infeasible restrictions. For example, a reversible process has to be carried out at an infinitely slow speed such that each thermodynamic parameter can adjust to its new equilibrium state. This implies that in a process where heat is transferred, the temperature difference between both bodies is zero. However, this is not possible in any real-world application. Also, even in lab-settings working at the molecular level, a true reversible process cannot be achieved as they are always completed in a finite time (Norton, 2016).

Because of these reasons, any heat engine is considered to be thermodynamically irreversible, although they remain functionally reversible in most cases. However, a reversible heat engine can still be designed, although be it just in theory (Norton, 2016). Nonetheless, this theoretical heat engine is very useful in evaluating real-world heat engines. The perfectly thermodynamically reversible heat engine provides an upper-limit for the maximum efficiency of a specific heat engine in a real world setting. This perfect heat engine is called the Carnot engine (Dass, 2021).

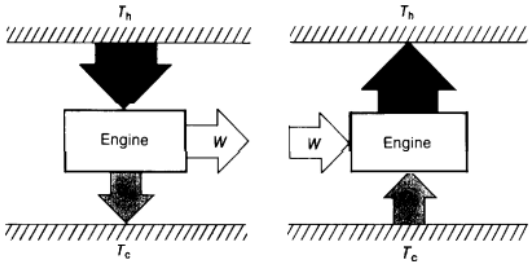

Figure 23: Heat engine as prime mover (left) and as heat pump (right)

A.b. The Carnot cycle and Second-law analysis

The Carnot cycle is an idealised thermodynamic cycle that determines the maximum efficiency of any thermodynamic heat engine. The cycle was first proposed by a Sadi Carnot in 1824 in his work *Reflexions sur la Puissance Motrice du Feu* and was later on expanded upon further by other scientists such as William Thomson (Dass, 2021). The Carnot cycle plays a key role in the evaluation of all heat engines, as it provides a theoretical baseline to which the real-world heat engine is compared.

In order to determine the maximum efficiency of a heat engine, the Carnot cycle makes some key assumptions on the thermodynamic processes that occur in the heat engine. First, the Carnot process is a thermodynamically reversible process. As is discussed in the previous chapter, reversibility implies an infinitely slow process where every change in the system is an equilibrium change (Dass, 2021). Second, the heat reservoirs that the engine is using to transfer heat must be infinite such that it maintains a constant temperature while heat is extracted or transferred to the reservoirs (Moran, Shapiro, Boettner, & Bailey, 2010). And third, no losses due to the second-law of thermodynamics must occur (Ennio & Astolfi, 2016). The different stages of the cycle are shown chronologically in figures 24 & 25. Considering all the assumptions made, the different stages are characterized in the following manner:

- 1 – 2 : isothermal expansion (heat in)
- 2 – 3 : adiabatic expansion
- 3 – 4 : isothermal compression (heat out)
- 4 – 1 : adiabatic compression

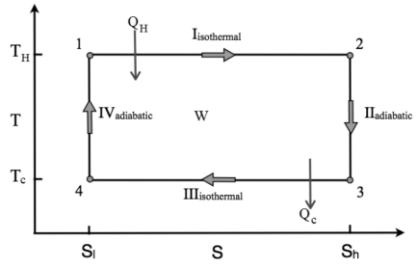

Figure 24: Carnot cycle T-s diagram (Abboud & Khoury, 2015)

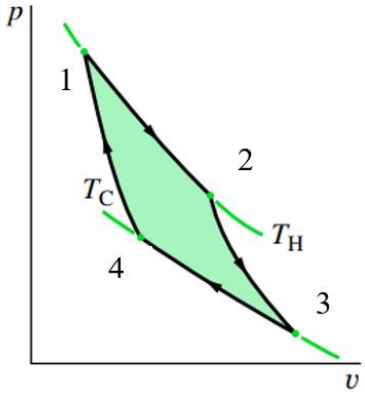

Figure 25: Carnot cycle p-v diagram (Moran, Shapiro, Boettner, & Bailey, 2010)

An important consequence of the Carnot cycle is the universal efficiency of the heat engine. Namely, the efficiency of a reversible ideal heat engine is determined completely by the temperatures of both thermal reservoirs (Dass, 2021). The efficiency of an ideal heat engine η_{rev} is given by its usefull energy output divided by its energy input. Thus, the ideal heat engine efficiency η_{rev} is expressed by:

$$\eta_{rev} = \frac{W}{Q_{Hot} - Q_{Cold}} = \frac{W}{Q_{net}} = 1 - \frac{T_{Cold}}{T_{Hot}}$$

Of course, the real-world heat engine based on these assumptions of the Carnot cycle does not exist. However, its definition is still very useful, for example when carrying out second-law analysis (Ennio & Astolfi, 2016).

Second-law analysis is a powerful tool for evaluating the efficiency of any power cycle because it creates a maximum-efficiency baseline. In short, the efficiency of any irreversible thermodynamic heat engine η_{irrev} is evaluated by calculating the calculating the Carnot efficiency of the cycle and subtracting all inefficiencies within the cycle $\Delta\eta_i$ (Ennio & Astolfi, 2016). Therefore, the cycle efficiency η_{rev} is expressed by:

$$\eta_{irrev} = \eta_{rev} - \sum_{i=1}^{n} \Delta\eta_i$$

$$With\ \Delta\eta_i = T * \sum_{i=1}^{n} \frac{\Delta S_i}{Q_{in}}$$

The inefficiencies $\Delta\eta_i$ within the cycle are caused by various irreversibilities, which are in turn the result of increases in entropy ΔS_i (Ennio & Astolfi, 2016). As the second law of thermodynamics states, any transfer of heat in a closed system must lead to an increase of the total entropy of that system (Dass, 2021). And, any real-world process that experiences an internal entropy increase is also non-reversible and will be less efficient than a theoretical process that does not experience this increase in internal entropy. These increases in entropy therefore reduce the overall thermodynamic efficiency of any thermodynamic heat cycle (Ennio & Astolfi, 2016).

The most important types of thermodynamic irreversibilities for heat engines are: friction, free expansion of a liquid and heat transfer with a finite temperature difference. (Moran, Shapiro, Boettner, & Bailey, 2010). All these irreversible processes are present in a typical heat engine, and thus by extension also in the organic Rankine cycle. This makes it impossible to make a real-world Carnot heat engine.

A.c. The Rankine cycle

The Rankine cycle (RC) is an idealized thermodynamic cycle that transforms heat into mechanical work, using steam as the working fluid (Ohji & Haraguchi, 2017). In other words, it is a prime mover real-world heat engine (Norton, 2016). From the Rankine cycle, the organic Rankine cycle is derived. Therefore, to fully understand the organic Rankine cycle, the Rankine cycle is also discussed. In the following chapters, the differences between the organic and the standard Rankine cycle are examined further. And, the advantages and disadvantages of ORC relative to RC are discussed.

In the Rankine cycle, super-heated steam is allowed to expand adiabatically through a turbine in order to carry out mechanical work. At the exhaust of the turbine, the steam is cooled down significantly due to expansion and it becomes saturated water vapour. Next, the saturated vapour is transformed into water by evaporating a coolant inside the condenser. Afterwards, the condensed water is pressurized up to the boiler pressure. Then, the boiler heats up the condensate up to the initial super-heated steam state using different heat exchangers, such as the economizer (or recuperator), evaporator and superheater. Finally, the super-heated steam expands again through a turbine, allowing for the cyclic behaviour of this thermodynamical process (Ohji & Haraguchi, 2017) (Badr, S., & P., 1985).

It is plain to see that the Rankine cycle also experiences irreversibilities and thus cannot achieve the Carnot efficiency (Ennio & Astolfi, 2016). Some key irreversibilities in the cycle are the free expansion of gas in the turbine, the transfer of heat in the boiler and condenser with a finite non-zero temperature difference and the friction of the fluids in the pump and piping of the installation.

The different stages of the cycle are shown chronologically in figures 26 & 27. Considering an idealised Rankine cycle, the different stages are characterized in the following manner:

- 1 – 2 : adiabatic expansion of steam
- 2 – 3 : isobaric condensation of steam into water
- 3 – 4 : isentropic compression of water
- 4 – 5 : isobaric heating of water in economizer
- 5 – 6 : isobaric evaporation of water into steam
- 6 – 1 : isobaric super-heating of steam in super-heater

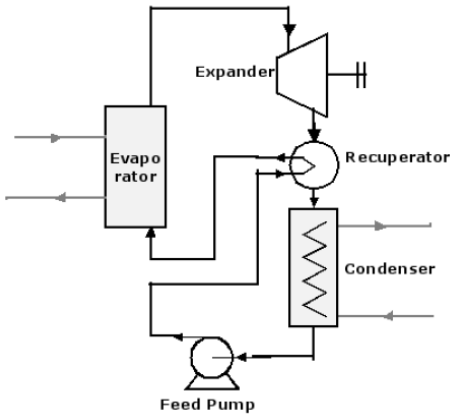

Figure 26: Rankine cycle schematic (Quoilin S. , 2011)

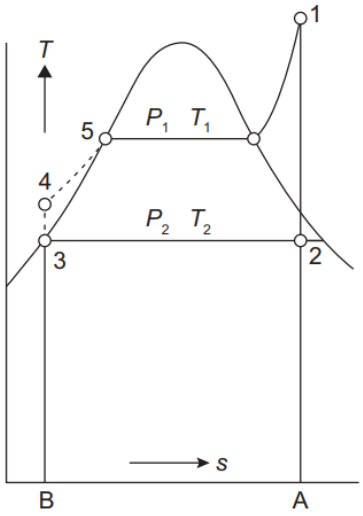

Figure 27: Rankine cycle T-s diagram (Ohji & Haraguchi, 2017)

Finally, there are two important remaining observations of the Rankine cycle that are clearly shown in figure 6. First, steam is super-heated before it is allowed to expand in the turbine. Super-heating is required as low quality steam that contains a relatively high percentage of vapour at during the expansion will cause erosion and wear in the turbine blades (Bahrami M. , 2020). And second, an economizer is used to heat the water before it is evaporated into steam. The economizer is a heat exchanger that transfers excess heat from the steam of turbine outlet to the water in the boiler. The inclusion of an economizer improves the overall efficiency of the system, because less heat energy is dissipated into the cold sink (Ohji & Haraguchi, 2017).

B. Working fluids

B.a. ODP and GWP

Previous generations of working fluids used in organic Rankine cycles (and also predominantly used in cooling processes) have done significant damage to the earth's Ozone layer in the past century (Bahrami, Pourfayaz, & Kasaeian, 2022). A reduction of the earth's Ozone layer in turn lead to increased UV radiation levels which caused increases in skin cancers, a higher prevalence of eye cataracts and more immune deficiency disorders. In addition, high UV radiation also damaged aquatic and terrestrial eco systems (European Comission, 2023). Furthermore, working fluids have also contributed in a non-negligible manner to global warming. For example, refrigerants such as CFC, HFCs and HCFCs are highly potent with a global warming potential that is thousands times greater than that of carbon dioxide (Bahrami, Pourfayaz, & Kasaeian, 2022). Therefore, the current generation of working fluids used in a newly designed ORC must adhere to more strict environmental standards, to ensure that ORC systems remain a useful tool in helping to build a more sustainable energy future. According to the new standards, a good working fluid must have zero ODP and a GWP lower than 150 (Bahrami, Pourfayaz, & Kasaeian, 2022). The zero ODP requirement is a direct consequence of the Montreal Protocol of 1987 instituted by the UN. This protocol has been amended 6 more times, each time enforcing more strict ODP requirements and also reducing the average GWP of fluids by e.g. banning the use of the most potent working fluids such as the HFCs (UN Environment Programme, 2023).

B.b. Other environmental considerations

Parameters such as the acidification potential (AP) and the eutrophication potential (EP) are also examined when comparing the environmental impact of fluids. The parameter AP indicates how much the fluid contributes to the acidification of rain. The parameter EP indicates to what level the fluid contributes to the over-fertilization of water and soil, resulting in undesirable levels of growth in biomass (Bahrami, Pourfayaz, & Kasaeian, 2022).

B.c. Techno-economic selection of working fluids

The financial feasibility of an ORC is a key parameter in any design, however, most research tends to focus on thermodynamic efficiency rather than financial efficiency. Still, in recent years, authors are starting to bridge this gap in the literature and using a more thermo-economic approach to analyse ORC's. In this kind of approach, the full cost of the installation using a specific working fluid is considered. The full cost difference between different working fluids is driven by the difference in operating costs, maintenance cost, working fluid price, operating pressure, inlet temperatures, temperature pinch, pump efficiency and turbine efficiency. Especially higher condenser pressures have a greater impact on overall financial costs. In general, a reduction in volumetric flow rate at the expander exhaust relates to the most cost savings. However, more detailed analysis is necessary for any specific context to determine better design guidelines (Desai & Bandyopadhyay, 2016) (Garg, Orosz, & Kumar, 2016).

A comparison of the main characteristics of a selection of common working fluids which are used in ORC systems is presented in table 5. The table shows that the modern standard concerning ODP and GWP is achievable (keeping the ODP at 0 and the GWP below 150). However, it also shows that working fluids are usually highly flammable and that toxicity is a relevant parameter to consider. The thermo-economic efficiencies of some working fluids compared by Desai & Bandyopadhyay are shown in table 6. The most straightforward parameter to interpret is the LCOE. LCOE is the Levelized Cost of Energy and should be used to compare different working fluids' total financial cost (Desai & Bandyopadhyay, 2016).

Table 5: Comparison of working fluids' main characteristics (Bahrami, Pourfayaz, & Kasaeian, 2022)

WF	ODP	GWP	t_c [K]	p_c [bar]	ρc [kg/m^3]	ASHRAE safety group	ASHRAE flammability	ASHRAE toxicity	Compatible lubricants
R-170 (ethane)	0	6	305.17	48.72	206.18	A3	Yes (Highly flammable)	No	MO, AB, POE
R-290 (propane)	0	3	369.74	42.51	220.48	A3	Yes (Highly flammable)	No	MO, AB, POE
R-1150 (ethylene)	0	4	282.2	50.41	214.24	A3	Yes (Highly flammable)	No	MO, AB, POE
R-600a (isobutane)	0	3	407.66	36.29	225.5	A3	Yes (Highly flammable)	No	MO, AB, POE
R-1270 (propylene)	0	2	364.06	45.55	229.63	A3	Yes (Highly flammable)	No	MO, AB, POE
n-hexane	0	3	507.739	30.31	232.8	A3	Yes (Highly flammable)	Toxic	–
R-E170 (dimethylether)	0	3	400.15	53.405	277	A3	Yes (Highly flammable)	No	SUNOCO 3GS
isopentane	0	11	461	33.81	235.92	A3	Yes (Highly flammable)	Toxic	MO, POE
neopentane	0	20	433.8	31.963	231.88	–	Yes (Highly flammable)	Toxic	–
n-butane	0	3	425	38	227.83	A3	Yes (Highly flammable)	Acceptable toxicity	PAG, POE
cyclohexane	0	–	554	40.7	274.36	A3	Yes (Highly flammable)	Acceptable toxicity	–
benzene	0	–	562	48.9	304.63	–	Flammable	Relatively non-toxic	–
toluene	0	3	593	41	292.08	B3	Yes (Highly flammable)	Toxic	–
cyclopropane	0	86	398.3	55.79	259.75	A3	Yes (Highly flammable)	Asphyxiant gas	MO
CO_2	0	1	304.19	7.38	40.8	A1	No	No	–

Table 6: Comparison of working fluids' thermo-economic efficiency (Desai & Bandyopadhyay, 2016)

Working fluid	P_{eva} (MPa)	P_{cond} (MPa)	T_{cond} (°C)	LFR based CSP plant						
				T_{5a} (°C)	A_p (m^2)	η_{cycle} (%)	Energy term (kWh/kW·y)	Economic term ($/kW·y)	Ratio of energy and economic term (1/LCOE') (kWh/$)	Actual LCOE ($/kWh)
R113	2.839	0.0929	45	202	15,176	20.8	1,883	450	4.184	0.353
Hexane	2.308	0.0451	45	216	13,428	21.81	1,884	477	3.953	0.373
Isohexane	2.308	0.0608	45	206	14,002	20.87	1,886	478	3.949	0.373
HMDS	1.186	0.0142	45	215	12,978	22.6	1,887	491	3.846	0.383
Benzene	3.583	0.0298	45	264	11,832	25.01	1,878	492	3.816	0.387
Cyclohexane	3.229	0.0300	45	262	11,651	25.43	1,875	500	3.748	0.393
OMTS	0.882	0.0050	66.6*	260	12,577	23.64	1,880	519	3.624	0.405
Water	4.0	0.0096	45	250	20,348	15.01	1,846	532	3.472	0.422
Pentane	2.45	0.1361	45	176	16,523	17.54	1,888	552	3.421	0.427
Toluene	3.154	0.0099	45	297	10,616	28.14	1,872	590	3.172	0.460
Heptane	2.087	0.0153	45	248	11,809	25.02	1,881	601	3.127	0.467
R245fa	2.128	0.2945	45	125	24,335	11.75	1,896	640	2.964	0.488

C. Other ORC energy sources

C.a. Concentrated solar power

Concentrated solar power concentrates the radiation of the sun via mirrors or lenses into a collector. The radiation energy from the sun is captured in the collector and is transformed into heat. The heat is then either converted into electricity using a power cycle (such as an ORC) or is stored in a thermal energy storage unit (Zhang, Baeyens, Degrève, & Cacères, 2013). This method of solar power collection is often compared to the use of photovoltaic solar panels (PV). In this method, sun light is directly transformed into electricity by allowing electrons in the photovoltaic panel to absorb energy from the photons of the available sun light, and create a DC current.

In CSP, the energy that is captured by the collector comes in the form of heat, which allows for easy and relatively efficient storage of large quantities of energy. However, in a PV power system energy, storage is difficult as the use of batteries for large quantities of energy becomes difficult and very expensive. Another advantage of CSP over PV power systems is that CSP outputs AC current through a generator that is attached to the rotating shaft of the turbine, whereas PV systems output DC. AC is generally preferred in power systems as it is easier to connect them to the grid that operates on AC. The DC power of photovoltaics can be converted into near-AC power using inverters, however, a pure and stable sine wave in practice is not achieved (Allessandra, 2023).

Still, PV power systems are significantly more popular then CSP, with about 400 GW installed global power of solar PV and only 8.1 GW of CSP in 2023 (International Energy Agency, 2024) (SolarPACES, 2024). One of the reasons that there is this significant difference is the higher initial cost of investment in CSP

relative to PV power. Furthermore, the efficiency of CSP is impacted more by the geographical location of the installed power plant relative to PV power. Although both power systems have a higher yield when they are located closer the equator, CSP's efficiency experiences greater efficiency losses when moved away from it. And, because most of the world's investments in solar power are made with capital from countries that are located further way from the equator, it may give an additional motivation to why PV is preferred over CSP on a global level. Nonetheless, when conditions are optimal, CSP outperforms PV when looking at power generation of large-scale power plants relative to their life-cycle costs (Ahmadi, et al., 2018).

The temperatures that the solar collector reaches in a CSP system varies significantly, depending on the location of the plant, the weather and the angle at which the sunlight reaches the mirrors. The temperature of the hot source of CSP which can be used in a power cycle ranges from about 230 – 600 °C (IRENA: International Renewable Energy Agency, 2012). Although some can even reach temperatures up to 1000°C (Ferrara, Gimelli, & Lunogo, 2014). These temperatures often exceed the working temperature ranges of a typical ORC. Still ORC technology is used, either alongside a Rankine cycle when dealing with high temperatures or directly when dealing with lower temperatures.

C.b. Waste heat

Waste heat is an important applications of the ORC technology and its relative importance continues to increase in recent years. Waste heat is the heat that is produced by a machine or process and that comes as the byproduct of doing work. As follows from the second law of thermodynamics, waste heat is inevitable because a share of the used heat energy must always be transferred to the cold sink (Dass, 2021). Still, this waste heat that is transferred to the cold source can still be made useful in an ORC, using it as the hot source for its cycle. A typical ORC installation installed for waste heat recovery in an industrial setting has an electrical power output in the range of 1 to 20 MW and is able to operate in a temperature range from 90°C to about 400°C (Exergy-ORC, 2022).

The potential of waste heat as a significant electrical energy source is clear. The industrial waste heat of Europe is estimated to be in a range of 200-300 TWh/year (Kosmadakis, 2024) (Papapetrou, Kosmadakis, Cipollina, La Commare, & Micale, 2018). About 65% of this waste heat is omitted in a temperature range of 100-400°C, which is applicable in a waste heat ORC. And about 35% is omitted at temperatures greater than 400°C. When waste heat is reapplied, it is often used directly in other industrial processes that require heat to operate or to heat homes and other buildings. Although direct use of heat is more efficient, waste heat can also be used to power an ORC and generate electricity. From the available waste heat potential, it is estimated that about 20-38 TWh/year in electrical energy of European industrial waste heat can easily be recovered using an ORC (Campana, et al., 2013) (Kosmadakis, 2024).

The most dominant industries in waste heat production in Europe in descending order are the iron & steel industry, non-metallic mineral industry, the paper and print industry, the non-ferrous metal industry and the chemical industry. These industries combined represent more than 95% of all industrial waste heat that is produced in the EU (Kosmadakis, 2024).